1 **CCN activity and organic hygroscopicity of aerosols downwind of an urban region in cen-**

2 **tral Amazonia: Seasonal and diel variations and impact of anthropogenic emissions**

4 Ryan Thalman[1,#], Suzane S. de Sá[2], Brett B. Palm[3], Henrique M. J. Barbosa[4], Mira L. Pöhlker[5],

5 M. Lizabeth Alexander[7], Joel Brito[4*], Samara Carbone[4], Paulo Castillo[1], Douglas A. Day[3],

6 Chongai Kuang[1], Antonio Manzi[8], Nga Lee Ng[9,10], Arthur J. Sedlacek III[1], Rodrigo Souza[11],

7 Stephen Springston[1], Thomas Watson[1], Christopher Pöhlker[5], Ulrich Pöschl[5,6], Meinrat O. An-

8 dreae[5,12], Paulo Artaxo[4] Jose L. Jimenez[3], Scot T. Martin[2,13], Jian Wang[1]

10 [1]Environmental and Climate Sciences Department, Brookhaven National Laboratory, Upton,

11 NY, USA

12 [2]School of Engineering and Applied Sciences, Harvard University, Cambridge, MA, USA

13 [3]Department of Chemistry and Biochemistry and Cooperative Institute for Research in Environ-

14 mental Sciences (CIRES), University of Colorado Boulder, Boulder, CO, USA

15 [4]Physics Institute, University of São Paulo, São Paulo, Brazil

16 [5]Biogeochemistry and Multiphase Chemistry Departments, Max Planck Institute for Chemistry,

17 Mainz, Germany

18 [6]Scripps Institution of Oceanography, University of California San Diego, La Jolla, CA, USA

19 [7]Pacific Northwest National Laboratory, Richland, WA, USA

20 [8]National Institute of Amazonian Research, Manaus, Amazonas, Brazil

21 [9]School of Chemical and Biomolecular Engineering, Georgia Institute of Technology, Atlanta,

22 GA, USA

23   [10]School of Earth and Atmospheric Sciences, Georgia Institute of Technology, Atlanta, GA,

24   USA

25   [11] Amazonas State University, Manaus, Amazonas, Brazil

26   [12]Scripps Institution of Oceanography, University of California San Diego, La Jolla, CA, USA

27   [13]Department of Earth and Planetary Sciences, Harvard University, Cambridge, MA, USA

29   [#]Now at Department of Chemistry, Snow College, Richfield, UT, USA

30   [*]Now at Laboratory for Meteorological Physics, University Clermont Auvergne, Clermont-

31   Ferrand, France

32   Correspondence to: J. Wang (jian@bnl.gov)

33 Abstract

35   During the *Observations and Modeling of the Green Ocean Amazon* (GoAmazon2014/5)

36 campaign, size-resolved cloud condensation nuclei (CCN) spectra were characterized at a re-

37 search site (T3) 60 km downwind of the city of Manaus, Brazil, in central Amazonia for one year

38 (12 March 2014 to 3 March 2015). Particle hygroscopicity (κ_{CCN}) and mixing state were derived

39 from the size-resolved CCN spectra, and the hygroscopicity of the organic component of the aer-

40 osol (κ_{org}) was then calculated from κ_{CCN} and concurrent chemical composition measurements.

41 The annual average κ_{CCN} increased from 0.13 at 75 nm to 0.17 at 171 nm, and the increase was

42 largely due to an increase in sulfate volume fraction. During both wet and dry seasons, κ_{CCN}, κ_{org},

43 and particle composition under background conditions exhibited essentially no diel variations.

44 The constant κ_{org} of ~ 0.15 is consistent with the largely uniform and high O:C value (~0.8), in-

45 dicating that the aerosols under background conditions are dominated by the aged regional aero-

46 sol particles consisting of highly oxygenated organic compounds. For air masses strongly influ-

47 enced by urban pollution and/or local biomass burning, lower values of κ_{org} and organic O:C

48 atomic ratio were observed during night, due to accumulation of freshly emitted particles, domi-

49 nated by primary organic aerosol (POA) with low hygroscopicity, within a shallow nocturnal

50 boundary layer. The O:C, κ_{org}, and κ_{CCN} increased from the early morning hours and peaked

51 around noon, driven by the formation and aging of secondary organic aerosol (SOA) and dilution

52 of POA emissions into a deeper boundary layer, while the development of the boundary layer,

53 which leads to mixing with aged particles from the residual layer aloft, likely also contributed to

54 the increases. The hygroscopicities associated with individual organic factors, derived from PMF

55 analysis of AMS spectra, were estimated through multi-variable linear regression. For the SOA

56 factors, the variation of the κ value with O:C agrees well with the linear relationship reported

57   from earlier laboratory studies of SOA hygroscopicity. On the other hand, the variation in O:C of

58   ambient aerosol organics is largely driven by the variation in the volume fractions of POA and

59   SOA factors, which have very different O:C values. As POA factors have hygroscopicity values

60   well below the linear relationship between SOA hygroscopicity and O:C, mixtures with different

61   POA and SOA fractions exhibit a steeper slope for the increase of κ_{org} with O:C, as observed

62   during this and earlier field studies. This finding helps better understand and reconcile the differ-

63   ences in the relationships between κ_{org} and O:C observed in laboratory and field studies, there-

64   fore providing a basis for improved parameterization in global models, especially in a tropical

65   context.

66

1 Introduction

Atmospheric aerosols have a major impact on the radiative balance of the Earth's climate system by changing the microphysical structure, lifetime, and coverage of clouds. For the same liquid water content, high aerosol concentration leads to more, smaller cloud droplets, and therefore higher cloud albedo (Twomey, 1977). The smaller droplet size also delays or inhibits warm precipitation, leading to increases in both cloud lifetime and coverage (Albrecht, 1989), and ultimately invigoration of convective clouds (Rosenfeld et al., 2008). Currently, the effects of aerosol on clouds remain one of the largest uncertainties in simulated climate change during industrial era, and a large portion of this uncertainty is due to the natural aerosol properties and processes represented in models (Carslaw et al., 2013; Ghan et al., 2013). The Amazon represents more than half of the planet's rainforest and is a rapidly changing region where deforestation, human activity and natural resource needs are all at play in changing the ecosystem (Andreae et al., 2015; Batistella et al., 2013; Davidson et al., 2012). The Amazon basin also represents at times one of the cleanest continental regions on the planet where it is still possible to find extended periods of little or no impact of anthropogenic activity, although the long-distance transport of pollution is occasionally observed (Andreae et al., 2015; Hamilton et al., 2014; Martin et al., 2010b; Wang et al., 2016a; Wang et al., 2016b; Williams et al., 2002). This makes the Amazon Basin an ideal location to characterize aerosol under near natural conditions and assess the impact due to urban emissions and biomass burning (Kuhn et al., 2010). The biogenic activity of this region makes it a major source of organic carbon released into the atmosphere via isoprene and monoterpenes (Guenther et al., 2006; Guenther et al., 2012; Kesselmeier et al., 2002; Kuhn et al., 2007) which are mediated by biotic stress through heat, sunlight and changes in CO_2 (Heald et al., 2009).

90   To understand the impact of aerosol on clouds and climate requires knowledge of the concen-

91   tration of cloud condensation nuclei, which are particles that are able to form cloud droplets un-

92   der relevant atmospheric conditions. The minimum supersaturation required to activate a particle

93   into a cloud droplet can be predicted using κ-Köhler theory based on particle size and the single

94   hygroscopicity parameter κ, which combines a number of thermodynamic properties required for

95   the description of water activity of the growing droplets (Petters and Kreidenweis, 2007). The

96   value of κ is determined by the physicochemical properties of the solutes, including their molar

97   volume, activity coefficient, and the effect on surface tension. For multi-component particles, κ

98   is the volume average of participating species. Hygroscopicity also describes particle growth un-

99   der sub-saturated conditions and can be derived from the particle growth factor (GF). However,

100   particles sometime exhibit larger κ values for droplet activation (derived from CCN measure-

101   ments under supersaturated conditions) than for particle growth (derived from particle GF under

102   sub-saturated conditions) (e.g., Duplissy et al., 2008; Good et al., 2010; Mikhailov et al., 2013;

103   Pajunoja et al., 2015; Wex et al., 2009). In this paper, "hygroscopicity" represents κ associated

104   with droplet activation derived from CCN measurements unless noted otherwise.

105   The hygroscopicities of typical inorganics in ambient particles are relatively well known.

106   However, atmospheric aerosols consist of a large number of organic compounds, which often

107   dominate the total fine aerosol mass (e.g., Zhang et al., 2007). The hygroscopicity of aerosol or-

108   ganics (κ_{org}) have been examined in both laboratory (e.g., Asa-Awuku et al., 2009; Duplissy et

109   al., 2011; King et al., 2009; Lambe et al., 2011; Massoli et al., 2010; Prenni et al., 2007;

110   Raymond and Pandis, 2003) and field studies (e.g., Cerully et al., 2015; Chang et al., 2010;

111   Dusek et al., 2010; Gunthe et al., 2009; Jimenez et al., 2009; Lathem et al., 2013b; Mei et al.,

112   2013a; Mei et al., 2013b; Moore et al., 2011; Moore et al., 2012; Pöhlker et al., 2016; Rose et al.,

113   2010; Shantz et al., 2008; Wang et al., 2008). Overall, these studies show that aerosol organics

114   exhibit a wide range of κ values from 0 to ~0.3, and κ_{org} often increases substantially during aer-

115   osol aging in the atmosphere (e.g., Duplissy et al., 2011; Jimenez et al., 2009; Lambe et al.,

116   2011; Massoli et al., 2010; Mei et al., 2013a).

117   A number of recent studies examined the sensitivity of predicted CCN concentration and

118   cloud droplet number concentration to aerosol properties (e.g., Ervens et al., 2010; Kammermann

119   et al., 2010; McFiggans et al., 2006; Mei et al., 2013a; Reutter et al., 2009; Rissman et al., 2004;

120   Roberts et al., 2002; Wang, 2007; Wang et al., 2008). These studies show that the predicted CCN

121   concentration is often sensitive to κ_{org}, especially for aerosol under background conditions where

122   organics tend to dominate submicron aerosol mass (Liu and Wang, 2010; Mei et al., 2013a). Us-

123   ing a constant κ_{org} may lead to large biases in predicted CCN concentrations and aerosol indirect

124   forcing (Liu and Wang, 2010). Therefore, it is imperative to understand organic hygroscopicity

125   under background conditions, such as in the Amazon forest, as well as the variation of organic

126   hygroscopicity due to anthropogenic emissions.

127   There have been several studies of aerosol hygroscopicity in the Amazon Basin over the past

128   20 years (Gunthe et al., 2009; Mikhailov et al., 2013; Pöhlker et al., 2016; Rissler et al., 2006b;

129   Roberts et al., 2001; Vestin et al., 2007; Whitehead et al., 2016; Zhou et al., 2002) . Gunthe et al.

130   (2009) performed size resolved CCN measurements during the wet season in February and

131   March 2008 as part of the AMAZE-08 campaign (Martin et al., 2010a). That study reported no

132   diel cycle in the CCN concentration during periods with little or no influence of pollution.

133   Pöhlker et al. (2016) measured size-resolved CCN spectra at a remote background site (Amazon

134   Tall Tower Observatory ATTO) over a one-year period from March 2014 to February 2015 and

135   observed no diel cycle and only weak seasonal trends in derived particle hygroscopicity, while

136   CCN concentrations had a pronounced seasonal cycle as the background aerosol concentration

137   was strongly influenced by regional biomass burning during the dry season. During the SMOCC-

138   2002 campaign (Large scale Biosphere atmosphere experiment in Amazonia – SMOke, aerosols,

139   Clouds, rainfall, and Climate) particle hygroscopicity was derived from HTDMA measurements

140   in the state of Rondônia in the southwest of the Amazon region during the dry season from Sep-

141   tember to November of 2002 (Rissler et al., 2006b; Vestin et al., 2007). The study concluded that

142   the diel variation in the aerosol hygroscopicity could be linked to the structure and dynamics of

143   the boundary layer. Local sources dominated night-time aerosol properties with downward mix-

144   ing from the residual layer aloft as the day progressed. All of these studies found that particle

145   hygroscopicity increased with particle size (from the Aitken to accumulation modes), consistent

146   with higher sulfate content at larger sizes (Gunthe et al., 2009). The same boundary layer evolu-

147   tion has been found to influence particle number and CCN evolution in a number of other related

148   studies (Fisch et al., 2004; Martin et al., 2010a; Rissler et al., 2006b; Vestin et al., 2007;

149   Whitehead et al., 2010; Zhou et al., 2002).

150   In this study we present measurements of size resolved CCN spectra at five particle diame-

151   ters ranging from 75 to 171 nm downwind of Manaus, Brazil, in central Amazonia for a period

152   of one year from March 12, 2014 to March 3, 2015. Particle hygroscopicity, mixing state, and

153   organic hygroscopicity are derived from the size-resolved CCN activated fraction and concurrent

154   aerosol composition measurements. The diel variations of these properties are examined for dif-

155   ferent seasons (i.e., wet season, dry season, and transition seasons) and for different types of rep-

156   resentative air masses, including background conditions, as well as influences of urban pollution

157   plumes and/or local biomass burning. During the wet season, the background air mass represents

158   near natural conditions, with occasional impact from anthropogenic emissions, while in the dry

159   season, the background is dominated by regional biomass burning aerosol particles. The relation-

160   ship between organic hygroscopicity and particle oxidation level (i.e., O:C atomic ratio) is exam-

161   ined for both dry and wet seasons. Hygroscopicities associated with organic factors from Aerosol

162   Mass Spectrometry (AMS) Positive Matrix Factorization (PMF) analysis are derived, and their

163   relationship with the O:C ratio is compared with those from previous laboratory studies.

164   **2 Experimental Setup**

165   **2.1 Measurement Sites**

166   *Observations and Modeling of the Green Ocean Amazon* (GoAmazon2014/5), sponsored by

167   the US Department of Energy (DOE) and several Brazilian and German agencies, took place at

168   multiple surface sites surrounding Manaus, Brazil, from January 2014 through December 2015

169   (Martin et al., 2016b). This work focuses on the measurements carried out at a downwind site

170   (T3, 3°12'47.82"S, 60°35'55.32"W, 60 km west of Manaus) from March 2014 to March 2015.

171   Depending on the wind direction, the T3 site experienced conditions ranging from nearly natural

172   to heavily polluted. More detailed characterizations of aerosol and gas phase chemical composi-

173   tion were carried out at the T3 site during Intensive Operating Periods (IOPs) from February 1,

174   2014 to March 31, 2014 and from August 15, 2014 to October 15, 2014. In addition, data from

175   two sites normally upwind of Manaus are also used in this study. These background sites include

176   the T0a site, (ATTO, 2° 8'47.88"S, 59° 0'18.00"W) (Andreae et al., 2015) and the T0t site,

177   (2.6091°S, 60.2093°W) (Martin et al., 2010a).

2.2 Activated Fraction of size-selected Particles

178

179   The CCN activation fraction of size-selected particles was measured using a Differential

180   Mobility Analyzer (DMA) coupled to a condensation particle counter (CPC, TSI Inc., 3010) and

181   a cloud condensation nuclei counter (CCNC, Droplet Measurement Technologies, Boulder, CO)

182   (Frank et al., 2006; Mei et al., 2013a; Moore et al., 2010; Petters et al., 2007). Aerosol particles

183   were sampled with a total flow rate (Q_a) of 1.53 L min^{-1} from a height of 5 m above ground level

184   and were dried to RH below 20% by a Nafion dryer immediately upon entering the instrument

185   container. The dried aerosol particles then reached steady state charge distribution inside a Kr-85

186   aerosol charger (TSI, model 3077A), prior to being introduced into the DMA operated with a

187   sheath flow rate (Q_{sh}) of 15.3 L min^{-1} to maintain a 10:1 sheath to aerosol flow ratio (Q_{sh}/Q_a).

188   The aerosol particles were size-selected by the DMA and the size-selected particles were simul-

189   taneously characterized by a CPC (Q_{CPC} = 0.53 L min^{-1}) and a CCNC (see Fig. S1 in the Sup-

190   plementary Information for further details). This system had been operated in previous field

191   campaigns by scanning the particle size while CCNC supersaturation was held constant (Mei et

192   al., 2013a; Mei et al., 2013b). During GoAmazon2014/5 the particle size classified by the DMA

193   was stepped through seven particle diameters (51, 75, 94, 112, 142, 171, and 222 nm), while the

194   CCNC supersaturation was also changed at each diameter by stepping the flow rates (Q_{CCN} rang-

195   ing from 0.2 to 1.0 L min^{-1}) and temperature gradient (ΔT = 4.5, 5.5, 6.5, 8.0 and 10.0°C). At a

196   given supersaturation, data were acquired for a minimum of 30 s and until 1500 particles were

197   counted by the CPC or up to a maximum time of 120 s. Depending on the aerosol number size

198   distribution, the measurement cycled through the seven particle sizes in 1 – 2 h (see Fig. S1 and

199   S2 for further details of the measurement setup and sampling protocol). The sampling sequence

200   was designed so that the change of CCNC supersaturation was mostly accomplished by stepping

201 flow rates, as the CCNC reaches steady state faster following flow changes than temperature

202 changes. Change of the temperature gradient was kept at a minimum frequency, but was neces-

203 sary given the wide range of supersaturation explored. Given the low particle number concentra-

204 tion (e.g., ~200 cm^{-3} under background conditions during the wet season), these approaches were

205 important to achieve adequate counting statistics with good time resolution to capture changes of

206 air mass within 10 – 20 minutes (Liu et al., 2016). The supersaturation of the CCNC was cali-

207 brated using ammonium sulfate aerosol, as described previously in the literature (e.g., Mei et al.,

208 2013a), at each operational set point (Q_{CCN} and ΔT), ranging from 0.075 – 1.1 %. Fluctuation of

209 the temperature inside the instrument container, ranging from 20 to 30°C over the course of a

210 day, led to substantial variation in the absolute temperature inside the CCNC growth chamber.

211 Calibrations were therefore repeated under a range of container and associated growth chamber

212 temperatures. The dependence of the supersaturation on the temperature at the top of CCNC col-

213 umn (instrument temperature T_1) was derived for each Q_{CCN} and ΔT pair and used to retrieve the

214 supersaturation over the range of the instrument operating conditions (see Fig. S3 and further

215 description in the Supplementary Information).

216 **2.3 Aerosol Chemical Composition**

217 Non-refractory sub-micron aerosol composition (organics, sulfate, nitrate, ammonium, and

218 chloride) was measured by a high-resolution time-of-flight aerosol mass spectrometer (HR-ToF-

219 AMS, Aerodyne Research Inc. (DeCarlo et al., 2006) during the two IOPs, and by an Aerosol

220 Chemical Speciation Monitor (ACSM, Aerodyne Research, Inc., Ng et al., 2011) from July 2014

221 to March 2015. The AMS sampled from an inlet equipped with a PM2.5 cyclone located at 5 m

222 above ground level. The ambient sample was first dried outside the container by a poly-tube

223 Nafion dryer (Perma Pure, model PD-100T). Once inside the container the sample was further

224   dried by a mono-tube Nafion dryer (Perma Pure, model MD-110) to achieve RH < 40% and was

225   split between the AMS and a Scanning Mobility Particle Sizer (SMPS, TSI, model 3081). Ambi-

226   ent measurements were obtained every 4 of 8 minutes. Further details of the AMS set up and op-

227   eration are described in de Sá et al. (2016).

228   The ACSM was a part of the Aerosol Radiation Measurement (ARM) Mobile Facility-1

229   (AMF-1) Mobile Aerosol Observation System (MAOS). Aerosol was sampled through an inlet

230   located 10 m above the ground. The aerosol sample was first dried through five large (40 x 1.75

231   cm I.D.) Nafion dryers before being distributed among various instruments including the ACSM.

232   The ACSM sampling alternated between with and without an in-line filter using a 3-way valve,

233   such that aerosol-free background could be subtracted from the ambient measurement. Twenty-

234   eight ambient and background scans of the quadrupole mass spectrometer (unit mass resolution)

235   were averaged to give one measurement every 30 min. The mass concentrations of organic spe-

236   cies, sulfate, nitrate, ammonium, and chloride were derived from measurements using approach-

237   es described in Ng et al. (2011).

238   Refractory black carbon (rBC) was measured using both a Single Particle Soot Photometer

239   (SP2, Droplet Measurement Technologies, Boulder, CO) and an aethalometer (Magee Scientific)

240   co-located with the AMS and ACSM. The SP2 measures rBC using laser-induced incandescence,

241   whereas the aethalometer measures equivalent black carbon (BC_e) (Andreae and Gelencsér,

242   2006) using light absorption from particles collected onto a filter. While these are fundamentally

243   different aerosol properties, both species (rBC and BC_e) were treated as equivalent in this study,

244   and BC_e concentration was adjusted to match that of rBC using the approach detailed in Section

245   2.2 of the Supplementary Information.

2.4 Additional Relevant Measurements

246

247   Additional measurements of aerosol microphysics, trace gas concentrations, and atmospheric

248   conditions used in this study are briefly described here. These measurements were part of the de-

249   ployment of the ARM AMF-1 facility during GoAmazon 2014/5 (Martin et al., 2016b). Relevant

250   aerosol measurements include dry particle number-size distributions from 10 to 480 nm by a

251   SMPS (TSI Inc. Model 3081) and the number concentration of particles with diameters greater

252   than 10 nm by a CPC (TSI Inc. Model 3772). Mixing ratios of CO and O_3 were characterized by

253   an Off-Axis Integrated Cavity Output Spectroscopy CO, N_2O and H_2O analyzer (model number

254   908-0014, Los Gatos) and UV Photometry O_3 analyzer (model 49i, Thermo Scientific Inc.), re-

255   spectively. Oxides of nitrogen (NO, NO_x, NO_2, NO_y) were measured using a chemiluminescence

256   technique (details given in Section S2.1 of the Supplementary Information). Meteorological data

257   included relative humidity (RH), ambient temperature, wind speed and direction, and rain accu-

258   mulation. The vertical profile of atmospheric backscatter (clouds and aerosol) and boundary lay-

259   er heights were estimated from ceilometer (model CL31,Vaisala) measurements.

260   **3 Methods**

261   **3.1 Derivation of Particle Hygroscopicity and Mixing State**

262   The particle hygroscopicity parameter, κ (Petters and Kreidenweis, 2007), was derived from

263   the activation spectrum (i.e., activated fraction as a function of supersaturation S) at the individu-

264   al particle sizes using approaches detailed in the literature (Bougiatioti et al., 2011; Cerully et al.,

265   2011; Lance et al., 2013; Mei et al., 2013a; Rose et al., 2008a). The activation spectrum of size-

266   selected particles was first corrected for the influence of multiply charged particles, which is es-

267   timated using the size distribution measured by the SMPS in MAOS and the activation spectrum

268   measured at the sizes of the doubly and triply charged particles (See Section S3.1). The corrected

269   activation spectrum of size selected particles was then fit with a cumulative lognormal (Mei et

270   al., 2013a; Rose et al., 2008b) functional form (See Fig. S6 for examples):

271    $$R_a(S) = \frac{E}{2}\left[1 + erf\left(\frac{\ln S - \ln S^*}{\sqrt{2\sigma_s^2}}\right)\right]$$ (1)

272   where R_a is the activated fraction as a function of supersaturation S, E is maximum activated

273   fraction, and $(1-E)$ represents the number fraction of particles consisting of only non-hygroscopic

274   species (e.g., uncoated rBC) that cannot serve as CCN under typical atmospheric supersatura-

275   tions. S^* is the supersaturation at which R_a reaches 50% of E, and represents the median critical

276   supersaturation of size-selected particles that serve as CCN. The value of σ_s is related to the slope

277   of the increasing R_a with S near S^* and reflects the heterogeneity of critical supersaturation,

278   which to a large degree arises from the heterogeneity of the hygroscopicity among size-selected

279   particles (Cerully et al., 2011; Mei et al., 2013a). The probability density function of hygrosco-

280   picity for size-selected particles is derived from the $R_a(S)$. The average hygroscopicity $\overline{\kappa_{CCN}}$ and

281   dispersion of the hygroscopicity $\sigma(\kappa)/\overline{\kappa_{CCN}}$ for the size-selected CCN were then derived from

282   the probability density function of hygroscopicity using the approach detailed in Section S3.4 in

283   Supplementary Information. The dispersion of the hygroscopicity reflects the composition heter-

284   ogeneity (i.e., mixing state) among size-selected particles (Mei et al., 2013a). For simplicity, we

285   use κ_{CCN} to represent the average hygroscopicity of size-selected CCN in the following sections.

3.2 Derivation of Organic Aerosol Hygroscopicity

286

287   The average particle hygroscopicity was then combined with the chemical composition data

288 to derive the hygroscopicity of the organic component of the size-selected particles, κ_{org}. Collec-

289 tively, the AMS, ACSM, SP2, and aethalometer provided mass concentrations of organic spe-

290 cies, sulfate, nitrate, ammonium, and rBC. The concentration of chloride was negligible (<<1%

291 of aerosol mass) and was not included in the analysis. Given the low concentrations during

292 GoAmazon 2014/5, size-resolved mass concentrations at the time resolution of the CCN meas-

293 urement were not directly derived from AMS particle time of flight (PToF) mode data. For IOP

294 1, measurements were classified into three groups based on bulk organic mass fraction and the

295 characteristic mass size distribution of each species was averaged from measurements in each

296 group. For the dry season, the measurements were classified into three groups each for day and

297 night periods based on the bulk aerosol organic mass fraction, and the mass size distribution of

298 each species was averaged from measurements in each of the six groups. The size-resolved mass

299 concentrations of sulfate, nitrate, and organics at the time resolution of the CCN measurement

300 were then derived by scaling the total mass concentration using the average mass size distribu-

301 tions for the corresponding group (based on the bulk organic mass fraction) of either wet or dry

302 season (de Sá, 2017). The shape of the NH_4^+ mass size distribution was assumed to be the same

303 as that of sulfate, as ammonium cations were primarily associated with sulfate. rBC was as-

304 sumed to have the same size distribution shape as the total aerosol mass (i.e., mass fraction of

305 rBC was independent of particle size); though this assumption may not always be appropriate,

306 the effect is expected to be very small as the monthly average volume fraction of rBC was al-

307 ways less than 4% (Fig. 1). A detailed description of the derivation of the size-resolved mass

308 concentrations is given in Section S4.1.

309   In most cases, NH_4^+ was insufficient to completely neutralize SO_4^{2-}. The concentrations of

310   both organonitrate and inorganic nitrate during the two IOPs were retrieved from AMS data

311   based on the ratio of ions NO^+ and NO_2^+ (de Sá, 2017; Fry et al., 2009). When the inorganic ni-

312   trate mass concentration was negligible (i.e., less than 30 ng m^{-3}), as in most of the cases, the

313   contributions of ammonium sulfate and ammonium bisulfate were calculated based on the mass

314   concentrations of SO_4^{2-} and NH_4^+ (Nenes et al., 1998). In rare cases when the mass concentra-

315   tion of inorganic nitrate was greater than 30 ng m^{-3}, sulfate was assumed to be ammonium sul-

316   fate. During non-IOP periods, only the total nitrate mass concentration is available, all nitrate

317   was assumed to be organonitrate (Cerully et al., 2015; Lathem et al., 2013a; Nenes et al., 1998;

318   Zhang et al., 2005), and sulfate fully neutralized by ammonium (see Section S4.2 in the Supple-

319   ment for a sensitivity study of these assumptions for non-IOP periods). The $-ONO_2$ portion of

320   the organonitrate was added back to the organic mass. We note that the amount of $-ONO_2$ added

321   back was typically small given the low mass fraction of nitrate in the aerosol. Cloud condensa-

322   tion nuclei were assumed to be internal mixtures of $(NH_4)_2SO_4$, NH_4HSO_4, NH_4NO_3, organics,

323   and rBC, and the volume fractions of the species were derived from the mass concentrations and

324   densities. Densities of organics were estimated from the ratios of O:C and H:C measured by the

325   AMS (Kuwata et al., 2012) and were on average 1450 ± 100 and 1470 ± 80 kg m^{-3} for IOP1 and

326   IOP2, respectively. Densities of 1770, 1790, 1730, 1800 kg m^{-3} were used for $(NH_4)_2SO_4$,

327   NH_4HSO_4, NH_4NO_3, and rBC (Bond and Bergstrom, 2006; Park et al., 2004), respectively. In

328   very rare cases, E was less than 100%, suggesting some of the size-selected particles were non-

329   hygroscopic. The non-hygroscopic particles were assumed to consist entirely of rBC (Mei et al.,

330   2013a). The volume concentration of the non-hygroscopic particles was derived as the product of

331   ($1-E$) and the total volume concentration (i.e., the sum of volume concentrations of organics,

332   (NH$_4$)$_2$SO$_4$, NH$_4$HSO$_4$, NH$_4$NO$_3$ and rBCs) at the size classified by the DMA. The volume con-

333   centration of rBC internally mixed within the CCN-active particles was then calculated as the

334   difference between the total rBC volume concentration and the volume concentration of the non-

335   hygroscopic particles. (Mei et al., 2013a; Mei et al., 2013b). Assuming a κ value of zero for rBC,

336   we can derive the hygroscopicity of the organic component of the CCN κ_{org} as:

337    $$\kappa_{org} = \frac{1}{x_{org}}\left(\kappa_{CCN} - x_{(NH_4)_2SO_4}\kappa_{(NH_4)_2SO_4} - x_{NH_4HSO_4}\kappa_{NH_4HSO_4} - x_{NH_4NO_3}\kappa_{NH_4NO_3}\right)$$ (2)

338   where x_i is the volume fraction of the respective species. The κ values are 0.61, 0.7 and 0.67 for

339   (NH$_4$)$_2$SO$_4$, NH$_4$HSO$_4$, and NH$_4$NO$_3$, respectively (Petters and Kreidenweis, 2007). The uncer-

340   tainty in κ_{org} using these calculations has been derived using the approach detailed in earlier

341   studies (Mei et al., 2013a; Mei et al., 2013b) and is on the order of 0.01 – 0.02 (which was gen-

342   erally between 10 and 20%) for this data set.

343   **3.2.1 Derivation of κ for AMS PMF Factors**

344   PMF was applied to the AMS mass spectra (Lanz et al., 2008; Ulbrich et al., 2009), and six

345   organic factors were identified for each of the two IOPs (de Sá, 2017). For IOP2 the PMF analy-

346   sis included data from 24 August to 15 October 15, 2014, excluding a major regional biomass

347   burning event from 16 to 23 August, which was treated separately in the PMF analysis. For IOP1

348   (wet season), the six factors were isoprene-epoxydiol-derived secondary organic aerosol (IE-

349   POX-SOA), more-oxidized oxygenated organic aerosol (MO-OOA, i.e., highly oxidized organ-

350   ics), less-oxidized oxygenated organic aerosol (LO-OOA), biomass burning organic aerosol

351   (BBOA) with characteristic peaks at m/z = 60 and 73 and correlated with the concentrations of

352   levoglucosan and vanillin, a factor with high contribution from m/z = 91 (Fac91) and correlated

353   with anthropogenic emissions of aromatics, and hydrocarbon-like organic aerosol (HOA). The

354   six factors for IOP2 included IEPOX-SOA, MO-OOA, LO-OOA, an aged biomass burning or-

355   ganic aerosol factor (aged-BBOA), a fresh biomass burning organic aerosol factor (fresh-

356   BBOA), and HOA. Further details of PMF analysis and the characteristics of the factors can be

357   found in de Sá (2017). The O:C ratio and calculated density for each factor are presented in Ta-

358   ble 1. In this study, the O:C ratio was derived using Improved-Ambient Method (Canagaratna et

359   al., 2015).

360   For each IOP, hygroscopicities associated with the six factors were attributed based on multi-

361   linear regression of κ_{org} with respect to the volume fractions of the factors (Levenberg-Marquardt

362   algorithm, IGOR Pro, Wavemetrics):

363    $$\kappa_{org} = \sum_{i}^{n} \kappa_i x_i \qquad\qquad (3)$$

364   where κ_i and x_i are the hygroscopicity and volume fraction of the individual organic PMF factors.

365   The volume fraction was derived from mass concentrations and the densities of the factors. κ_{org}

366   represents the average organic hygroscopicity at particle diameters (D_p) of 142 and 171 nm. As

367   the PMF analysis is based on the mass spectra of the bulk sub-micrometer aerosol (i.e., MS mode

368   measurements), an implicit assumption of Eq. (3) is that the bulk volume fractions of the factors

369   represented those over the sizes at which κ_{org} was derived (i.e., D_p = 142 and 171 nm). The va-

370   lidity of this assumption is discussed in the results section. The robustness of the factor hygro-

371   scopicity derived through linear regression depends on the variation of the factor volume fraction

372   during the measurement period. The HOA hygroscopicity was assumed as zero based on the re-

373   sults from previous studies (Cappa et al., 2009; Cappa et al., 2011; Jimenez et al., 2009), and the

374   hygroscopicity of the other five factors were derived by multilinear regression as described

375   above.

376   **3.3 Classification of Seasons and Air Masses**

377   The one-year sampling period was divided into different seasons by grouping months accord-

378   ing to the similarity of the aerosol properties and trace gas concentrations measured at the two

379   background sites, T0a and T0t, as well as monthly accumulated rainfall. In this study, the sea-

380   sons were defined as follows: the first wet season: March, April and May of 2014; the first tran-

381   sition season: June and July 2014; the dry season: August and September of 2014; the second

382   transition season: October, November and the first half of December 2014; and the second wet

383   season: the second half of December 2014 and January, February and the first few days of March

384   2015.

385   For each season, the air masses arriving at the T3 site were classified into three different

386   types: background, urban pollution, and local biomass burning based on trace gas and aerosol

387   measurements at all sites. During the wet season, the background air mass represented near natu-

388   ral conditions, with occasional impact from anthropogenic emissions, while in the dry season, the

389   background was dominated by regional biomass burning aerosol particles. Polluted air masses

390   represent those with strong influence from urban emissions, which were mostly from Manaus.

391   The local-biomass-burning type describes those air masses strongly influenced by local (i.e.,

392   fresh) biomass burning activities, which dominated over the impact from urban pollution, if any.

393   For each season, background conditions were identified when CO and CN concentrations were

394   below the thresholds derived from measurements at the background T0a and T0t sites, and the

395   NO$_y$ mixing ratio was below 1.5 ppb. Non-background conditions were identified by CN and CO

396   concentrations above the respective threshold levels. As biomass burning aerosol typically has a

397   higher fraction of accumulation mode particles, and the emissions from Manaus were more dom-

398   inated by Aitken mode particles, the fraction of particles with diameter less than 70 nm was used

399   to differentiate air masses strongly influenced by local biomass burning from those with more

400   impact from urban pollution (see Table S2 in Supplementary Information for details). Contami-

401   nation by the emissions from an on-site diesel generator, grass cutting activities, tractors, and

402   other vehicles were evidenced by rBC concentrations above 1.0 µg m^{-3} or CN concentration

403   above 10,000 cm^{-3}. Over the one-year measurement period, background, urban pollution, and

404   local biomass burning represented 12.4%, 38.5%, and 28.4% of the CCN measurements, respec-

405   tively (Table S3). We note that the air masses arriving at the T3 site often included contributions

406   from different sources. The classification of the air masses using the above three types clearly

407   represents a simplification, but is very helpful for understanding the properties of aerosols influ-

408   enced by the various major sources.

409   **4 Results**

410   **4.1 Seasonal Trend and Size Dependence of Hygroscopicity and Chemical Composition**

411   The monthly average κ_{CCN} at the T3 site varied from 0.1 to 0.2 at five particle diameters

412   ranging from 75 nm to 171 nm (Fig. 1a), and was substantially lower than the value of 0.3 ± 0.1

413   suggested for continental sites (Andreae and Rosenfeld, 2008). This was due to the large organic

414   volume fraction, up to 95% observed at the T3 site. In this study, measurements at 51 and 222

415   nm were not included, because the range of supersaturation sampled inside the CCN counter on-

416   ly adequately captured the activation spectrum for 51/222 nm particles with relatively high/low

417   κ_{CCN} values, leading to a positive/negative bias of the average κ_{CCN}. The value of κ_{CCN} exhibited

418   similar seasonal variations at all five sizes. During the transition from wet to dry season, κ_{CCN}

419   decreased by 20-30% with the absolute minimum of 0.116 occurring at 75 nm in September and

420   October (Fig. 1a).

421   The seasonal trend of κ_{CCN} was mainly driven by the variation of κ_{org}, which shows the low-

422   est value in September during the dry season (Fig. 1b). Despite a strong increase of aerosol mass

423   concentration from wet to dry season due to biomass burning emissions, the organic volume

424   fraction exhibited little season variation, and was ~90% or higher at the four sizes from 94 to

425   171 nm (Fig. 1c). A minor increase in organic volume fraction in October might have also con-

426   tributed to the lower κ_{CCN} value observed. The species volume fractions at 75 nm are not shown

427   due to the very low signal-to-noise ratio of the AMS PToF data in the small particle diameter

428   range. No clear seasonal trend was observed for sulfate volume fraction, which ranged from 3%

429   to 9% at the four sizes. Nitrate and rBC represented a small fraction of aerosol volume, and were

430   less than 1% and ~4%, respectively.

431   The average κ_{CCN} increased with increasing particle size for all three air mass types and dur-

432   ing all the seasons (Fig. 2), consistent with decreasing organic volume fraction with increasing

433   particle size (Fig. 1c). The κ_{CCN} at 75, 94, 112, 142, and 171 nm averaged for the one-year meas-

434   urement period were 0.130 ± 0.028, 0.144 ± 0.039, 0.148 ± 0.043, 0.164 ± 0.046, and 0.167 ±

435   0.042 respectively. The value of κ_{CCN} and its size dependence under background conditions were

436   largely consistent among different seasons, and were in good agreement with those observed un-

437   der near natural conditions during the AMAZE-08 campaign at T0t in the wet season (Gunthe et

438   al., 2009) and during the one-year period from March 2014 to February 2015 at the background

439   T0a site (Pöhlker et al., 2016). Compared to κ_{CCN}, κ_{org} was largely independent of particle size

440   for all three air mass types, indicating that the size dependence of κ_{CCN} was mainly due to the

441 size dependence of the organic volume fraction and particle composition (Fig. 1c – f). During

442 the dry season, aerosols classified as urban pollution and local biomass burning exhibited lower

443 κ_{org} values compared to background aerosols, contributing to the lower values of overall κ_{CCN}.

444 **4.2 Diel Trends of Particle and Organic Hygroscopicities**

445 The diel variations of aerosol properties are presented in Figs. 3-7 for different air masses

446 during the two IOPs. Aerosol properties derived from the size-resolved CCN measurements, in-

447 cluding κ_{CCN}, $\sigma_{\kappa_{CCN}} / \overline{\kappa}_{CCN}$, and κ_{org}, and the volume fractions of different species were averaged

448 at the three largest sizes (D_p = 112, 142, and 171 nm). The fraction of organic mass at m/z = 44

449 (f_{44}) and O:C were derived from the AMS bulk measurements. Also shown are diel variations of

450 planetary boundary layer height, CN, and aerosol volume concentrations based on 5-minute av-

451 erage data.

452 **4.2.1 Wet Season Aerosol**

453 *Background conditions*

454 Figures 3 and 4 show the diel variations of aerosol properties during the wet season of 2014

455 for background and urban pollution air masses, respectively. There were only 0.7% of data clas-

456 sified as local biomass burning (see Table S3), which is insufficient to evaluate the diel trends.

457 During the wet season, the background air mass represents near-natural conditions, with mini-

458 mum impact from anthropogenic emissions, although long-distance transport of African biomass

459 burning may contribute to the aerosols observed (Chen et al., 2009; Wang et al., 2016b). Back-

460 ground aerosol constantly exhibited relatively high hygroscopicity of ~0.19 throughout the day.

461 The lack of a diel trend in κ_{CCN} is also in agreement with the results from the T0a site (ATTO),

462   which is upwind of Manaus and served as a background site (Fig. 8). The particle composition

463   averaged for the three particles diameters was dominated by organics, representing ~ 90% of the

464   aerosol volume. The lack of a diel trend in κ_{CCN} and κ_{org} suggest little variation in particle com-

465   position throughout the day. The nearly constant κ_{org} of ~0.16 is also consistent with the lack of a

466   diel trend in f_{44} and O:C. The values of f_{44} and O:C are ~0.2 and ~0.8, respectively, indicating

467   that the aerosol under background condition during the wet season was dominated by the aged

468   regional aerosol particles consisting of highly oxygenated organic compounds.

469   Aerosol number and volume concentrations exhibited a minimum at ~310 cm^{-3} and ~0.3 μm^{3}

470   cm^{-3}, respectively, just before sunrise. The number and volume concentrations started increasing

471   after sun rise, and peaking at 400 cm^{-3} and 0.8 μm^{3} cm^{-3} in the afternoon. These diel variations

472   are partially attributed to the wet scavenging of accumulation mode particles, which dominate

473   the submicron particle concentrations under background conditions, and the mixing of the parti-

474   cles from the residual layer aloft down to the surface as the boundary layer develops in the morn-

475   ing. During the night, the radiative cooling at the surface leads to a shallow nocturnal boundary

476   layer with low and variable winds. RH near surface was near 100%, and fog or mist was identi-

477   fied by the weather station (Present Weather Detector, Visalia) 62% of the time during the one-

478   year measurement period. The gradual decrease of particle number and volume concentration

479   during these fog events were due to the wet deposition of the accumulation mode particles acti-

480   vated into droplets. Similar decreases of particle number concentration were previously reported

481   during night fog events in the tropical rainforest in Borneo (Whitehead et al., 2010). After sun-

482   rise, the boundary layer deepened on average from less than 200 up to 800 m as a result of solar

483   heating (Fig. 3g). Consequently, particles in the residual layer aloft (Fisch et al., 2004; Rissler et

484   al., 2006b), which were not impacted by the fog, were mixed down to the surface, leading in part

485   to the observed increases in both number and volume concentrations. Such mixing of particles

486   from the residual layer in the morning had been observed previously in the Amazon basin during

487   the dry season (Rissler et al., 2006a). The formation of secondary organic aerosol (SOA) as a

488   result of photochemical oxidation (in both gas and particle phases) likely contributed to the in-

489   crease in volume concentration (Chen et al., 2015; Chen et al., 2009; Martin et al., 2010a; Pöschl

490   et al., 2010).

491   ***Air masses impacted by urban pollution***

492   Air masses arriving at the T3 site frequently had passed over urban and industrial areas up-

493   wind. When the air mass was influenced by the urban pollution, κ_{CCN} and its dispersion exhibited

494   clear diel variations (Fig. 4). The value of κ_{CCN} was lower during the night at 0.15, and it in-

495   creased from the early morning hours, peaking at a value of 0.19 around noon (local time, UTC –

496   4 h). The dispersion was anti-correlated with κ_{CCN}, exhibiting higher values (i.e., increased het-

497   erogeneity in particle chemical composition) during night and a minimum value around noon. To

498   a large degree, the diel trend of κ_{CCN} was due to the variation of κ_{org}. The value of κ_{org} was lower

499   during night at 0.10 and increased to 0.16 at noon. The increase of κ_{org} is consistent with the var-

500   iation of O:C, which increased during the early morning and reached the highest value of 0.8

501   around noon time. The pollution strongly affected the particle number and volume concentra-

502   tions, both exhibiting similar diel trends. Under polluted conditions, particle number concentra-

503   tion ranged on average from 1500 to 2300 cm^{-3}, an increase by a factor of ~5 from that under

504   background conditions. In comparison, the increase of the volume concentration was only about

505   a factor of 2 (i.e., from a range of 0.3 - 0.75 to 1.0 to 1.3 μm^3 cm^{-3}), as the urban pollution is

506   dominated by Aitken mode particles that make a relatively small contribution to aerosol mass

507   and volume concentration.

508   The diel variations of κ_{CCN}, its dispersion, κ_{org}, and O:C are explained as follows. During

509   night, particles in freshly emitted pollution, which are dominated by primary organic aerosol

510   (POA) and have low hygroscopicity, are mixed with more aged particles within a shallow noc-

511   turnal boundary layer (Bateman et al., 2016). In the absence of photochemical oxidation and ag-

512   ing, this external mixture leads to higher dispersion of particle hygroscopicity, as well as overall

513   lower O:C and κ_{org}. As the pollution aerosols are mainly from isolated point sources, they are

514   confined in the shallow nocturnal boundary layer during night, and the residual layer above the

515   T3 site is expected to consist of aged background aerosols. Therefore, unlike under background

516   conditions, the mixing of aerosol aloft in the residual layer down to the surface cannot by itself

517   explain the increase in particle number and volume concentration during the day, both of which

518   were substantially above the background values. These increases under polluted conditions might

519   be due to the stronger urban influence at T3 during the day. The strong increase of CN concen-

520   tration at 16:00 UTC (local time 12:00) could be caused by the arrival at the T3 site of the Ma-

521   naus plume emitted during early morning traffic hours. To a large degree, the increases in O:C

522   and κ_{org} are due to the formation and aging of SOA in the pollution, while the development of the

523   daytime boundary layer, which leads to dilution of pollution and mixing with aged particles from

524   the residual layer, can also contribute to the increases. The condensation of secondary species

525   and photochemical aging also lead to more homogenous composition among particles (Mei et al.,

526   2013a), and therefore lower dispersion of κ_{CCN}, as was observed. The O:C reached a maximum

527   average value of 0.8, similar to that under the background conditions. This suggests that the for-

528   mation and photochemical aging of SOA quickly led to highly oxygenated organic compounds

529   (i.e. within several hours) (de Sá, 2017).

4.2.2 Dry Season Aerosol

Background conditions

Figures 5-7 show the diel variations of the aerosol properties observed during the dry season

for background, urban pollution, and local biomass burning air masses, respectively. During the

dry season, the background aerosol (Fig. 5) is strongly influenced by regional biomass burning,

and air masses arriving at the T3 site often pass through urban and industrial areas along the

Amazon River and in northeast Brazil (Andreae et al., 2015), indicating that the background aer-

osol is also impacted by more aged urban and industrial emissions (Martin et al., 2016a). Despite

different aerosol sources and processes, the particle hygroscopicity, dispersion, and κ_{org} exhibited

similar values as those of background aerosol during the wet seasons, and a lack of obvious diel

variations. This is also consistent with the absence of a significant diel trend of κ_{CCN} observed at

T0a (ATTO) during the dry season (Fig. 8). The O:C value increased slightly from 0.8 during

night to 0.9 in the afternoon, possibly due to further oxidation and aging of background aerosols

during the day time. The high value of O:C is consistent with the relatively high value of κ_{org}

(0.15) and is close to that observed under background condition during the wet season, indicating

highly oxygenated organic aerosol. The number and volume concentrations were lower just be-

fore dawn and increased during the early morning, again a result of wet scavenging of particles

by fog followed by the mixing of aerosol aloft in the residual layer down to the surface as the

boundary layer develops in the morning.

Air masses impacted by urban pollution and local biomass burning

For urban pollution (Fig. 6) and local biomass burning (Fig. 7) air masses during the dry sea-

son, κ_{CCN} (urban pollution: 0.12 – 0.20, local biomass burning: 0.10 – 0.17), its dispersion (urban

552   pollution: 0.4 – 1.0, local biomass burning: 0.4 – 0.9), κ_{org} (urban pollution: 0.10 – 0.15; local

553   biomass burning: 0.08 – 0.14), and O:C (polluted: 0.7 – 0.85; biomass burning: 0.7 – 0.86)

554   showed similar values and diel variations as those under polluted conditions during the wet sea-

555   son. This is consistent with the picture that freshly emitted particles (in either the case of urban

556   pollution or local biomass burning) lead to overall lower O:C, κ_{org}, and higher κ_{CCN} dispersion

557   during night, followed by increases in O:C, κ_{org}, and a decrease in the dispersion during day time,

558   which are mainly driven by the formation and photochemical aging of SOA, with contributions

559   from the mixing of background aerosol aloft in the residual layer down to the surface and dilu-

560   tion of fresh emission as the boundary layer develops. Compared to urban pollution, local bio-

561   mass burning air masses exhibited lower κ_{CCN} and κ_{org} values during night and stronger diel vari-

562   ations. In the afternoon, κ_{org} and O:C reached high values of 0.14 and 0.86, respectively, as ob-

563   served for background aerosols.

564   For urban pollution air masses, aerosol number and volume concentrations showed similar

565   trends for both seasons. The increases of number and volume concentration from early morning

566   to noon were similar, about 1000 cm^{-3} and 0.5 $\mu m^3/cm^3$, respectively, for both wet and dry sea-

567   sons. The percentage increases were less pronounced in the dry season due to the higher back-

568   ground values. In contrast to urban pollution, local biomass burning showed higher aerosol num-

569   ber and volume concentrations at night, and decreased during the morning. Local biomass burn-

570   ing activities typically peaked during evening hours, consistent with frequent classification of the

571   night time aerosol as local biomass burning (Fig. 7i) (Vestin et al., 2007). Despite the wet re-

572   moval of particles by fog, the strong emission from local biomass burning, largely confined with-

573   in the shallow nocturnal boundary layer, led to higher surface aerosol concentrations than those

574   in the residue layer aloft, which likely represented the regional background. As the boundary

575 layer deepened in the morning, the mixing with aerosol from the residual layer led to decreases

576 in both aerosol number and volume concentration observed at the surface (Fig. 7e,f).

4.3 Hygroscopicity of PMF Factors and the Variation of Organic Hygroscopicity with Oxi-

dation Level

579 The hygroscopicities associated with the AMS PMF factors were estimated through multi-

580 variable linear regression using different subsets of the data, as well as the entire dataset for each

581 of the two IOPs (IOP1 in Fig. 9 and IOP2 in Fig. 10). The different subsets included measure-

582 ments during day, night, certain sampling periods, and ranges in particle hygroscopicity disper-

583 sion. Comparison of the hygroscopicities derived from the different subsets of data allowed us to

584 examine the robustness of this approach. Uncertainty in the derived κ for individual factors was

585 determined by the number of points available to fit in the time series, with greater data coverage

586 and therefore lower uncertainty during the dry season. For the wet season (IOP1), the hygrosco-

587 picity associated with PMF factors derived using different subsets of the data are largely in

588 agreement with those derived from the entire dataset. There are notable differences between the

589 hygroscopicities of MO-OOA and Fac91 factors derived using data under background conditions

590 only and those derived using the entire dataset. Such difference could be partially due to the lim-

591 ited data under the background conditions during IOP1 (Fig. 3). For the dry season (IOP2), the

592 hygroscopicities of PMF factors derived using measurements under background conditions or

593 data with hygroscopicity dispersion less than 0.4 are quite different from those derived using

594 other data subsets and the entire dry season dataset. The agreement among the PMF factor hy-

595 groscopicities derived using different sub datasets during the wet season and the disagreements

596 for the dry season are attributed to the applicability of the underlying assumption that the bulk

597 volume fractions of PMF factors (i.e., derived from MS mode data) represented those at the sizes

598   of CCN measurements. For the wet season, the average f_{44} was largely independent of particle

599   size from 130 to 400 nm (Fig. S10), the size range that dominated bulk aerosol mass concentra-

600   tion measured by AMS. This is consistent with the assumption that the bulk volume fractions of

601   the PMF factors represent those at the two CCN sizes (142 and 171 nm). For the dry season, the

602   f_{44} averaged over local biomass burning air masses and the entire IOP2 exhibited an increase

603   with particle diameter from 100 to 300 nm (Fig. S10). For periods with hygroscopicity dispersion

604   less than 0.4 or under background conditions, the average size distribution of f_{44} was noisier due

605   to fewer data points. Nevertheless, the size distribution shows f_{44} was largely independent of the

606   particle size under these conditions, consistent with the assumption described above. In the fol-

607   lowing discussion, we focus on the PMF factor hygroscopicities derived using all data during the

608   wet season, and under background conditions in the dry season.

609   The MO-OOA factors for the two IOPs exhibit very similar O:C and κ values. The O:C val-

610   ues were 1.19 and 1.24, and κ values were 0.20 and 0.21 for IOP1 and 2, respectively (Table 1).

611   The O:C and κ values are consistent with those of some typical SOA compounds, such as malo-

612   nic acid, which has an O:C value of 1.33 and a κ value of 0.23 (Kumar et al., 2003), and succinic

613   acid, which has an O:C value of 1 and a κ value of 0.23 (Hori et al., 2003). For the LO-OOA and

614   IEPOX-SOA factors, the hygroscopicities vary between the two IOPs. The κ of IEPOX-SOA

615   were 0.18 and 0.08 during IOP1 and IOP2, respectively, and the κ of LO-OOA factor varied

616   from 0.12 to 0.20 between IOP 1 and IOP 2. The difference in κ may be partially due to the

617   change of O:C values of the factors derived for the two IOPs. Difference in SOA precursors and

618   therefore composition in LO-OOA (Ng et al., 2010) may also contribute to the difference in its κ

619   values between the two IOPs. The variation of IEPOX-SOA κ between the two IOPs could be a

620   result of the different RH conditions, which may strongly influence the composition of IEPOX-

621   SOA (Riva et al., 2016).

622   During the wet season, a factor with high contribution from $m/z = 91$ (Fac91) was identified.

623   The Fac91 factor correlates with several tracers for anthropogenic emissions, including NO_x,

624   benzene, toluene, trimethylbenzene (TMB) and xylenes, but not high NO_x isoprene products (e.g.

625   methylglyceric acid) (de Sá, 2017). This factor likely represents SOA formed from aromatics

626   emitted from urban areas, possibly combined with a mixture of freshly oxidized biogenic com-

627   pounds within the urban-influenced air (de Sá, 2017). The Fac91 factor has a hygroscopicity val-

628   ue of 0.10, and a much lower O:C ratio of 0.328 compared to those of MO-OOA and LO-OOA.

629   Less oxidized organic factors identified by the PMF analysis were HOA of both IOPs,

630   BBOA of IOP1 and fresh and aged BBOA of IOP2. These factors represent primary OA (POA),

631   except that the aged BBOA of IOP2 likely included contributions from oxidized POA or SOA.

632   The hygroscopicity of the HOA factors was fixed as zero in the multivariate regressions. All

633   BBOA factors have a distinctive $m/z = 60$ peak and correlate with biomass burning traces includ-

634   ing levoglucosan and vanillin (de Sá, 2017). The retrieved hygroscopicity values for the BBOA

635   factors are substantially lower than those of SOA factors, especially for the fresh BBOA factor

636   during IOP2. The extremely low hygroscopicity suggests that the fresh BBOA, likely produced

637   by local fires, behaves very similar to HOA in term of CCN activation despite a substantially

638   higher O:C.

639   Figures 11 and 12 show that for SOA factors, including IEPOX-SOA, LO-OOA, MO-OOA

640   for both IOPs and Fac91 for IOP1, the κ value increases with increasing O:C, and the variation of

641   κ with O:C agrees with the linear relationship derived from laboratory studies of SOA CCN ac-

642   tivities (Lambe et al., 2011). The low hygroscopicity of the HOA and the BBOA factors, which

643   are below the linear relationship for SOAs, are also consistent with laboratory results of POA

644   and oxidized POA (Lambe et al., 2011). Cerully et al. (2015) derived κ of LO-OOA, MO-OOA,

645   and IEPOX-SOA factors from data collected in the southeast US during Southern Oxidant and

646   Aerosol Study (SOAS). A different name, Isoprene-OA, was used for the IEPOX-SOA factor in

647   Cerully et al. (2015), as while this factor is mainly attributed to SOA formed from IEPOX up-

648   take, it might not be entirely due to IEPOX (Schwantes et al., 2015; Xu et al., 2015a; Xu et al.,

649   2015b). The O:C values calculated using the Improved-Ambient method (Canagaratna et al.,

650   2015) are 0.59, 0.61, and 0.92 for the IEPOX-SOA, LO-OOA, and MO-OOA factors reported in

651   Cerully et al. (2015), respectively (personal communication, L. Xu and N.L. Ng). For the LO-

652   OOA, MO-OOA factors reported in Cerully et al. (2015), κ and O:C values are largely consistent

653   with the linear relationship between κ and O:C derived from Lambe et al. (2011). Cerully et al.

654   (2015) also reported IEPOX-SOA (i.e., called Isoprene-OA in their study) factor κ of 0.2, simi-

655   lar to 0.18 derived for IOP1. The O:C value of the IEPOX-SOA factor during the SOAS study

656   was 0.59, somewhat lower than those derived from both IOPs of GoAmazon. While the IEPOX-

657   SOA factors identified using different datasets share many similar features, they are not identical

658   and can consist of different groups of compounds. Such differences may be due to varying de-

659   grees of oxidation in different environment between the two field campaigns.

660   For comparison with earlier field studies, the values of κ_{org} and O:C were averaged according

661   to the hours of the day over particle diameters of 142 and 171 nm for data under polluted condi-

662   tions during IOP1 and all data during IOP2 (Figs. 11 and 12). For the one-hour diel averages, the

663   slope of κ_{org} vs. O:C, derived through a bivariate least squares fit (i.e., Orthogonal distance re-

664   gression), is steeper than that derived from laboratory studies of SOA hygroscopicity, especially

665   during IOP2. This steep slope during IOP2 is consistent with the results from earlier field studies

666   (Mei et al., 2013b), although there is a clear offset between the two relationships. The O:C ratios

667   from Mei et al. (2013b) and Lambe et al. (2011) were scaled by a factor of 1.27 to account for

668   changes in the method of calculating the O:C ratio (Improved-Ambient, Canagaratna et al., 2015)

669   while all O:C values from this work were calculated using the Improved-Ambient method. This

670   offset between the field studies may be partially due to the different precursors of the SOA for

671   the campaigns, with higher anthropogenic VOC fraction expected for CalNex and CARES,

672   which took place near Los Angeles and Sacramento, respectively. In addition, biomass burning

673   represented a much smaller fraction of the organics during CalNex and CARES (Mei et al.,

674   2013a; Mei et al., 2013b). The factors associated with secondary processes (e.g., MO-OOA, LO-

675   OOA, and IEPOX-SOA), which have higher O:C values, exhibited higher volume fraction dur-

676   ing the day, whereas the factors associated with primary emissions (e.g. HOA and BBOA),

677   which have lower O:C, had higher volume fractions during the night (de Sá, 2017). As a result,

678   the diel trend of overall O:C was to a large degree driven by the variations in volume fractions of

679   the POA and SOA factors with very different O:C values. This is in contrast to laboratory stud-

680   ies, in which the increase of O:C was mainly driven by oxidation. As POA exhibits hygrosco-

681   picity values well below the linear fit between SOA hygroscopicity and O:C, mixtures with dif-

682   ferent POA and SOA fractions lead to a steeper slope for the increase of κ_{org} with O:C, as shown

683   by the results from this and previous field studies (Mei et al., 2013b).

684   **5 Conclusions**

685   Size-resolved CCN spectra at five particle diameters ranging from 75 to 171 nm were

686   characterized down-wind of Manaus, Brazil, in central Amazonia for a period of one year from

687   March 12, 2014 to March 3, 2015 during GoAmazon2014/5. For each season, the air masses ar-

688   riving at the site were classified into different types, including background, urban pollution, and

689   local biomass burning. During the wet season, the background air mass represented near natural

690   conditions, at times with impact from anthropogenic emissions, while in the dry season, the

691   background was dominated by regional and long-distance biomass burning aerosol particles. Pol-

692   luted air masses represented those with strong influence from urban emissions, which were most-

693   ly from Manaus. The local-biomass-burning type describes those strongly influenced by local

694   (i.e., fresh) biomass mass burning activities that dominate over the impact from urban pollution,

695   if any.

696   Particle hygroscopicity (κ_{CCN}), mixing state, and organic hygroscopicity (κ_{org}) were derived

697   from size-resolved CCN activation fraction and concurrent aerosol composition measurements.

698   The monthly mean κ_{CCN} exhibits the lowest values during the dry season, largely due to lower

699   κ_{org} when aerosol was often strongly influenced by local biomass burning. The κ_{CCN} increased

700   with particle size during all seasons, consistent with decreasing organic volume fraction with in-

701   creasing particle size. Under background conditions, the value of κ_{CCN} and its size dependence

702   were largely consistent among different seasons, despite the very different aerosol sources. Dur-

703   ing the dry season, aerosols classified as urban pollution and local biomass burning exhibited

704   lower κ_{org} values compared to background aerosols, contributing to the lower values of overall

705   κ_{CCN}.

706   Under background conditions during both wet and dry seasons, the largely constant diel

707   trends of κ_{CCN} and κ_{org} suggest little variation in particle composition throughout the day. The

708   constant κ_{org} of ~ 0.15 is consistent with the lack of a diel trend in f_{44} and O:C. The high values

709   of f_{44} and O:C indicate that the aerosols under background conditions are dominated by the aged

710   regional aerosol particles consisting of highly oxygenated organic compounds. When the air

711   mass is influenced by urban pollution or local biomass burning, κ_{CCN}, κ_{org}, f_{44}, and O:C exhibit

712   clear diel variations. The value of κ_{CCN} (0.1 - 0.2) is lower during the night, and increases from

713   the early morning hours, peaking around noon (local time, UTC - 4 h). This diel trend of κ_{CCN} is

714   largely driven by the variation in κ_{org} (0.08-0.15), consistent with the variation of O:C. The dis-

715   persion of κ_{CCN} is anti-correlated with κ_{CCN}, exhibiting higher values during night and a mini-

716   mum value around noon, indicating an increased heterogeneity in particle chemical composition

717   during night time. These diel variations for air masses strongly influenced by urban pollution and

718   local biomass burning indicate that during night, freshly emitted particles, dominated by POA

719   and with low hygroscopicity, are mixed with more aged particles within a shallow nocturnal

720   boundary layer. In the absence of photochemical oxidation and aging, this external mixture leads

721   to higher dispersion of particle hygroscopicity, as well as overall lower O:C and κ_{org}. The in-

722   creases in O:C and κ_{org} during daytime are driven by the formation and aging of SOA and dilu-

723   tion of POA emissions into a deeper boundary layer, while the development of the boundary lay-

724   er, which leads to mixing with aged particles from the residual layer, likley also contributes to

725   the increases.

726   The hygroscopicities associated with individual PMF organic factors were derived through

727   multi-variable linear regression. For the SOA factors, κ increases within increasing O:C, and the

728   variation of κ with O:C agrees well with the linear relationship derived from laboratory studies of

729   SOA hygroscopicity (Lambe et al., 2011). The low hygroscopicity of HOA and the BBOA fac-

730   tors, which are below the linear relationship, are also consistent with laboratory results of POA

731   and oxidized POA (Lambe et al., 2011). In contrast, the slope of κ_{org} (i.e., overall organic hygro-

732   scopicity) vs O:C is much steeper when compared to that derived from laboratory studies of

733   SOA hygroscopicity, especially for IOP2. Such difference is because the increase of O:C was

734   driven primarily by oxidation in laboratory SOA studies, while the variation in O:C of ambient

735   organics is to a large degree due to the variations in volume fractions of POA and SOA factors,

736   which have very different O:C values. As POA factors show hygroscopicity values well below

737   the linear fit between SOA hygroscopicity and O:C, mixtures with different POA and SOA frac-

738   tions lead to a steeper slope for the increase of κ_{org} with O:C, as shown by the results from this

739   and earlier field studies (Mei et al., 2013).

740

741

742 **Acknowledgements**

743 We acknowledge the support from the Central Office of the Large Scale Biosphere Atmosphere

744 Experiment in Amazonia (LBA), the National Institute of Amazonian Research (INPA), Amazo-

745 nas State University (UEA), and the Max Planck Society (MPG). The Office of Biological and

746 Environmental Research of the Office of Science of the United States Department of Energy is

747 acknowledged for funding, specifically the Atmospheric Radiation Measurement (ARM) Climate

748 Research Facility and the Atmospheric System Research (ASR) Program. The work was con-

749 ducted under scientific license 001030/2012-4 of the Brazilian National Council for Scientific

750 and Technological Development (CNPq). NLN acknowledged support from NSF grant 1242258

751 and US EPA STAR grant RD-83540301. This publication's contents are solely the responsibility

752 of the grantee and do not necessarily represent the official views of the US EPA. Further, US

753 EPA does not endorse the purchase of any commercial products or services mentioned in the

754 publication. PA and HB acknowledge the support from FAPESP under research grants

755 13/50510-5 and 13/05014-0, and from Royal Society under research grant NA 140450.

756

References

Albrecht, B. A.: Aerosols, Cloud Microphysics, and Fractional Cloudiness, Science, 245, 1227-1230, 1989.

Andreae, M. O., Acevedo, O. C., Araùjo, A., Artaxo, P., Barbosa, C. G. G., Barbosa, H. M. J., Brito, J., Carbone, S., Chi, X., Cintra, B. B. L., Silva, N. F. d., Dias, N. L., Dias-Júnior, C. Q., Ditas, F., Ditz, R., Godoi, A. F. L., Godoi, R. H. M., Heimann, M., Hoffmann, T., Kesselmeier, J., Könemann, T., Krüger, M. L., Lavric, J. V., Manzi, A. O., Moran-Zuloaga, D., Nölscher, A. C., Nogueira, D. S., Piedade, M. T. F., Pöhlker, C., Pöschl, U., Rizzo, L. V., Ro, C.-U., Ruckteschler, N., Sá, L. D. A., Sá, M. D. O., Sales, C. B., Santos, R. M. N. D., Saturno, J., Schöngart, J., Sörgel, M., Souza, C. M. d., Souza, R. A. F. d., H. Su, N., Targhetta, Tóta, J., Trebs, I., Trumbore, S., Eijck, A. v., Walter, D., Wang, Z., Weber, B., Williams, J., Winderlich, J., Wittmann, F., Wolff, S., and Yáñez-Serrano, A. M.: The Amazon Tall Tower Observatory (ATTO): overview of pilot measurements on ecosystem ecology, meteorology, trace gases, and aerosols, Atmos. Chem. Phys., 15, 10723-10776, 2015.

Andreae, M. O. and Gelencsér, A.: Black carbon or brown carbon? The nature of light-absorbing carbonaceous aerosols, Atmos. Chem. Phys., 6, 3131-3148, 2006.

Andreae, M. O. and Rosenfeld, D.: Aerosol–cloud–precipitation interactions. Part 1. The nature and sources of cloud-active aerosols, Earth-Science Reviews, 89, 13-41, 2008.

Asa-Awuku, A., Engelhart, G. J., Lee, B. H., Pandis, S. N., and Nenes, A.: Relating CCN activity, volatility, and droplet growth kinetics of beta-caryophyllene secondary organic aerosol, Atmos. Chem. Phys., 9, 795-812, 2009.

Bateman, A. P., Gong, Z., Harder, T. H., de Sá, S. S., Wang, B., Castillo, P., China, S., Liu, Y., O'Brien, R. E., Palm, B., Shiu, H.-W., Silva, G. d., Thalman, R., Adachi, K., Alexander, M. L., Artaxo, P., Bertram, A. K., Buseck, P. R., Gilles, M. K., Jimenez, J. L., Laskin, A., Manzi, A. O., Sedlacek, A., Souza, R. A. F., Wang, J., Zaveri, R., and Martin, S. T.: Anthropogenic influences on the physical state of submicron particulate matter over a tropical forest, 2016. submitted, 2016.

Batistella, M., Artaxo, P., Nobre, C., Bustamante, M., and Luizão, F.: Results from LBA and a Vision for Future Amazonian Research. In: Amazonia and Global Change, American Geophysical Union, 2013.

Bond, T. C. and Bergstrom, R. W.: Light Absorption by Carbonaceous Particles: An Investigative Review, Aerosol Science and Technology, 40, 27-67, 2006.

Bougiatioti, A., Nenes, A., Fountoukis, C., Kalivitis, N., Pandis, S. N., and Mihalopoulos, N.: Size-resolved CCN distributions and activation kinetics of aged continental and marine aerosol, Atmospheric Chemistry and Physics, 11, 8791-8808, 2011.

Canagaratna, M. R., Jimenez, J. L., Kroll, J. H., Chen, Q., Kessler, S. H., Massoli, P., Hildebrandt Ruiz, L., Fortner, E., Williams, L. R., Wilson, K. R., Surratt, J. D., Donahue, N. M., Jayne, J. T., and Worsnop, D. R.: Elemental ratio measurements of organic compounds using

795 aerosol mass spectrometry: characterization, improved calibration, and implications, Atmos.
796 Chem. Phys., 15, 253-272, 2015.

797 Cappa, C. D., Bates, T. S., Quinn, P. K., and Lack, D. A.: Source characterization from ambient
798 measurements of aerosol optical properties, Geophysical Research Letters, 36, n/a-n/a, 2009.

799 Cappa, C. D., Che, D. L., Kessler, S. H., Kroll, J. H., and Wilson, K. R.: Variations in organic
800 aerosol optical and hygroscopic properties upon heterogeneous OH oxidation, Journal of
801 Geophysical Research: Atmospheres, 116, n/a-n/a, 2011.

802 Carslaw, K. S., Lee, L. A., Reddington, C. L., Pringle, K. J., Rap, A., Forster, P. M., Mann, G.
803 W., Spracklen, D. V., Woodhouse, M. T., Regayre, L. A., and Pierce, J. R.: Large contribution of
804 natural aerosols to uncertainty in indirect forcing, Nature, 503, 67-71, 2013.

805 Cerully, K. M., Bougiatioti, A., Hite, J. R., Guo, H., Xu, L., Ng, N. L., Weber, R., and Nenes, A.:
806 On the link between hygroscopicity, volatility, and oxidation state of ambient and water-soluble
807 aerosols in the southeastern United States, Atmos. Chem. Phys., 15, 8679-8694, 2015.

808 Cerully, K. M., Raatikainen, T., Lance, S., Tkacik, D., Tiitta, P., Petäjä, T., Ehn, M., Kulmala,
809 M., Worsnop, D. R., Laaksonen, A., Smith, J. N., and Nenes, A.: Aerosol hygroscopicity and
810 CCN activation kinetics in a boreal forest environment during the 2007 EUCAARI campaign,
811 Atmos. Chem. Phys., 11, 12369-12386, 2011.

812 Chang, R. Y. W., Slowik, J. G., Shantz, N. C., Vlasenko, A., Liggio, J., Sjostedt, S. J., Leaitch,
813 W. R., and Abbatt, J. P. D.: The hygroscopicity parameter (κ) of ambient organic aerosol at a
814 field site subject to biogenic and anthropogenic influences: relationship to degree of aerosol
815 oxidation, Atmos. Chem. Phys., 10, 5047-5064, 2010.

816 Chen, Q., Farmer, D. K., Rizzo, L. V., Pauliquevis, T., Kuwata, M., Karl, T. G., Guenther, A.,
817 Allan, J. D., Coe, H., Andreae, M. O., Pöschl, U., Jimenez, J. L., Artaxo, P., and Martin, S. T.:
818 Submicron particle mass concentrations and sources in the Amazonian wet season (AMAZE-08),
819 Atmos. Chem. Phys., 15, 3687-3701, 2015.

820 Chen, Q., Farmer, D. K., Schneider, J., Zorn, S. R., Heald, C. L., Karl, T. G., Guenther, A.,
821 Allan, J. D., Robinson, N., Coe, H., Kimmel, J. R., Pauliquevis, T., Borrmann, S., Pöschl, U.,
822 Andreae, M. O., Artaxo, P., Jimenez, J. L., and Martin, S. T.: Mass spectral characterization of
823 submicron biogenic organic particles in the Amazon Basin, Geophysical Research Letters, 36,
824 n/a-n/a, 2009.

825 Davidson, E. A., de Araujo, A. C., Artaxo, P., Balch, J. K., Brown, I. F., C. Bustamante, M. M.,
826 Coe, M. T., DeFries, R. S., Keller, M., Longo, M., Munger, J. W., Schroeder, W., Soares-Filho,
827 B. S., Souza, C. M., and Wofsy, S. C.: The Amazon basin in transition, Nature, 481, 321-328,
828 2012.

829 de Sá, S. S.: Atmos. Chem. Phys. Discuss., in preparation, 2017.

830 de Sá, S. S., Palm, B. B., Campuzano-Jost, P., Day, D. A., Newburn, M. K., Hu, W., Isaacman-
831 VanWertz, G., Yee, L. D., Thalman, R., Brito, J., Carbone, S., Artaxo, P., Goldstein, A. H.,

832 Manzi, A. O., Souza, R. A. F., Mei, F., Shilling, J. E., Springston, S. R., Wang, J., Surratt, J. D.,
833 Alexander, M. L., Jimenez, J. L., and Martin, S. T.: Influence of urban pollution on the
834 production of organic particulate matter from isoprene epoxydiols in central Amazonia, Atmos.
835 Chem. Phys. Discuss., 2016, 1-58, 2016.

836 DeCarlo, P. F., Kimmel, J. R., Trimborn, A., Northway, M. J., Jayne, J. T., Aiken, A. C., Gonin,
837 M., Fuhrer, K., Horvath, T., Docherty, K. S., Worsnop, D. R., and Jimenez, J. L.: Field-
838 Deployable, High-Resolution, Time-of-Flight Aerosol Mass Spectrometer, Analytical Chemistry,
839 78, 8281-8289, 2006.

840 Duplissy, J., DeCarlo, P. F., Dommen, J., Alfarra, M. R., Metzger, A., Barmpadimos, I., Prevot,
841 A. S. H., Weingartner, E., Tritscher, T., Gysel, M., Aiken, A. C., Jimenez, J. L., Canagaratna, M.
842 R., Worsnop, D. R., Collins, D. R., Tomlinson, J., and Baltensperger, U.: Relating
843 hygroscopicity and composition of organic aerosol particulate matter, Atmos. Chem. Phys., 11,
844 1155-1165, 2011.

845 Duplissy, J., Gysel, M., Alfarra, M. R., Dommen, J., Metzger, A., Prevot, A. S. H., Weingartner,
846 E., Laaksonen, A., Raatikainen, T., Good, N., Turner, S. F., McFiggans, G., and Baltensperger,
847 U.: Cloud forming potential of secondary organic aerosol under near atmospheric conditions,
848 Geophys. Res. Lett., 35, L03818, 2008.

849 Dusek, U., Frank, G. P., Curtius, J., Drewnick, F., Schneider, J., Kürten, A., Rose, D., Andreae,
850 M. O., Borrmann, S., and Pöschl, U.: Enhanced organic mass fraction and decreased
851 hygroscopicity of cloud condensation nuclei (CCN) during new particle formation events,
852 Geophysical Research Letters, 37, n/a-n/a, 2010.

853 Ervens, B., Cubison, M. J., Andrews, E., Feingold, G., Ogren, J. A., Jimenez, J. L., Quinn, P. K.,
854 Bates, T. S., Wang, J., Zhang, Q., Coe, H., Flynn, M., and Allan, J. D.: CCN predictions using
855 simplified assumptions of organic aerosol composition and mixing state: a synthesis from six
856 different locations, Atmospheric Chemistry and Physics, 10, 4795-4807, 2010.

857 Fisch, G., Tota, J., Machado, L. A. T., Silva Dias, M. A. F., da F. Lyra, R. F., Nobre, C. A.,
858 Dolman, A. J., and Gash, J. H. C.: The convective boundary layer over pasture and forest in
859 Amazonia, Theor Appl Climatol, 78, 47-59, 2004.

860 Frank, G. P., Dusek, U., and Andreae, M. O.: Technical note: A method for measuring size-
861 resolved CCN in the atmosphere, Atmos. Chem. Phys. Discuss., 6, 4879-4895, 2006.

862 Fry, J. L., Kiendler-Scharr, A., Rollins, A. W., Wooldridge, P. J., Brown, S. S., Fuchs, H., Dube,
863 W., Mensah, A., dal Maso, M., Tillmann, R., Dorn, H. P., Brauers, T., and Cohen, R. C.: Organic
864 nitrate and secondary organic aerosol yield from NO3 oxidation of beta-pinene evaluated using a
865 gas-phase kinetics/aerosol partitioning model, Atmos. Chem. Phys., 9, 1431-1449, 2009.

866 Ghan, S. J., Smith, S. J., Wang, M. H., Zhang, K., Pringle, K. J., Carslaw, K. S., Pierce, J. R.,
867 Bauer, S. E., and Adams, P. J.: A simple model of global aerosol indirect effects, J. Geophys.
868 Res., 118, 6688-6707, 2013.

869 Good, N., Topping, D. O., Allan, J. D., Flynn, M., Fuentes, E., Irwin, M., Williams, P. I., Coe,
870 H., and McFiggans, G.: Consistency between parameterisations of aerosol hygroscopicity and
871 CCN activity during the RHaMBLe discovery cruise, Atmos. Chem. Phys., 10, 3189-3203, 2010.

872 Guenther, A., Karl, T., Harley, P., Wiedinmyer, C., Palmer, P. I., and Geron, C.: Estimates of
873 global terrestrial isoprene emissions using MEGAN (Model of Emissions of Gases and Aerosols
874 from Nature), Atmospheric Chemistry and Physics, 6, 3181-3210, 2006.

875 Guenther, A. B., Jiang, X., Heald, C. L., Sakulyanontvittaya, T., Duhl, T., Emmons, L. K., and
876 Wang, X.: The Model of Emissions of Gases and Aerosols from Nature version 2.1
877 (MEGAN2.1): an extended and updated framework for modeling biogenic emissions,
878 Geoscientific Model Development, 5, 1471-1492, 2012.

879 Gunthe, S. S., King, S. M., Rose, D., Chen, Q., Roldin, P., Farmer, D. K., Jimenez, J. L., Artaxo,
880 P., Andreae, M. O., Martin, S. T., and Poschl, U.: Cloud condensation nuclei in pristine tropical
881 rainforest air of Amazonia: size-resolved measurements and modeling of atmospheric aerosol
882 composition and CCN activity, Atmos. Chem. Phys., 9, 7551-7575, 2009.

883 Hamilton, D. S., Lee, L. A., Pringle, K. J., Reddington, C. L., Spracklen, D. V., and Carslaw, K.
884 S.: Occurrence of pristine aerosol environments on a polluted planet, Proceedings of the National
885 Academy of Sciences, 111, 18466-18471, 2014.

886 Heald, C. L., Wilkinson, M. J., Monson, R. K., Alo, C. A., Wang, G., and Guenther, A.:
887 Response of isoprene emission to ambient CO2 changes and implications for global budgets,
888 Global Change Biology, 15, 1127-1140, 2009.

889 Hori, M., Ohta, S., Murao, N., and Yamagata, S.: Activation capability of water soluble organic
890 substances as CCN, J. Aerosol Sci., 34, 419-448, 2003.

891 Jimenez, J. L., Canagaratna, M. R., Donahue, N. M., Prevot, A. S. H., Zhang, Q., Kroll, J. H.,
892 DeCarlo, P. F., Allan, J. D., Coe, H., Ng, N. L., Aiken, A. C., Docherty, K. S., Ulbrich, I. M.,
893 Grieshop, A. P., Robinson, A. L., Duplissy, J., Smith, J. D., Wilson, K. R., Lanz, V. A., Hueglin,
894 C., Sun, Y. L., Tian, J., Laaksonen, A., Raatikainen, T., Rautiainen, J., Vaattovaara, P., Ehn, M.,
895 Kulmala, M., Tomlinson, J. M., Collins, D. R., Cubison, M. J., Dunlea, E. J., Huffman, J. A.,
896 Onasch, T. B., Alfarra, M. R., Williams, P. I., Bower, K., Kondo, Y., Schneider, J., Drewnick, F.,
897 Borrmann, S., Weimer, S., Demerjian, K., Salcedo, D., Cottrell, L., Griffin, R., Takami, A.,
898 Miyoshi, T., Hatakeyama, S., Shimono, A., Sun, J. Y., Zhang, Y. M., Dzepina, K., Kimmel, J.
899 R., Sueper, D., Jayne, J. T., Herndon, S. C., Trimborn, A. M., Williams, L. R., Wood, E. C.,
900 Middlebrook, A. M., Kolb, C. E., Baltensperger, U., and Worsnop, D. R.: Evolution of Organic
901 Aerosols in the Atmosphere, Science, 326, 1525-1529, 2009.

902 Kammermann, L., Gysel, M., Weingartner, E., Herich, H., Cziczo, D. J., Holst, T.,
903 Svenningsson, B., Arneth, A., and Baltensperger, U.: Subarctic atmospheric aerosol composition:
904 3. Measured and modeled properties of cloud condensation nuclei, J. Geophys. Res., 115,
905 D04202 2010.

906 Kesselmeier, J., Kuhn, U., Rottenberger, S., Biesenthal, T., Wolf, A., Schebeske, G., Andreae,
907 M. O., Ciccioli, P., Brancaleoni, E., Frattoni, M., Oliva, S. T., Botelho, M. L., Silva, C. M. A.,

908   and Tavares, T. M.: Concentrations and species composition of atmospheric volatile organic
909   compounds (VOCs) as observed during the wet and dry season in Rondonia (Amazonia), J.
910   Geophys. Res., 107, 2002.

911   King, S. M., Rosenoern, T., Shilling, J. E., Chen, Q., and Martin, S. T.: Increased cloud
912   activation potential of secondary organic aerosol for atmospheric mass loadings, Atmos. Chem.
913   Phys., 9, 2959-2971, 2009.

914   Kuhn, U., Andreae, M. O., Ammann, C., Araújo, A. C., Brancaleoni, E., Ciccioli, P., Dindorf, T.,
915   Frattoni, M., Gatti, L. V., Ganzeveld, L., Kruijt, B., Lelieveld, J., Lloyd, J., Meixner, F. X.,
916   Nobre, A. D., Pöschl, U., Spirig, C., Stefani, P., Thielmann, A., Valentini, R., and Kesselmeier,
917   J.: Isoprene and monoterpene fluxes from Central Amazonian rainforest inferred from tower-
918   based and airborne measurements, and implications on the atmospheric chemistry and the local
919   carbon budget, Atmos. Chem. Phys., 7, 2855-2879, 2007.

920   Kuhn, U., Ganzeveld, L., Thielmann, A., Dindorf, T., Schebeske, G., Welling, M., Sciare, J.,
921   Roberts, G., Meixner, F. X., Kesselmeier, J., Lelieveld, J., Kolle, O., Ciccioli, P., Lloyd, J.,
922   Trentmann, J., Artaxo, P., and Andreae, M. O.: Impact of Manaus City on the Amazon Green
923   Ocean atmosphere: ozone production, precursor sensitivity and aerosol load, Atmos. Chem.
924   Phys., 10, 9251-9282, 2010.

925   Kumar, P. P., Broekhuizen, K., and Abbatt, J. P. D.: Organic acids as cloud condensation nuclei:
926   Laboratory studies of highly soluble and insoluble species, Atmos. Chem. Phys., 3, 509-520,
927   2003.

928   Kuwata, M., Zorn, S. R., and Martin, S. T.: Using Elemental Ratios to Predict the Density of
929   Organic Material Composed of Carbon, Hydrogen, and Oxygen, Environmental Science &
930   Technology, 46, 787-794, 2012.

931   Lambe, A. T., Onasch, T. B., Massoli, P., Croasdale, D. R., Wright, J. P., Ahern, A. T.,
932   Williams, L. R., Worsnop, D. R., Brune, W. H., and Davidovits, P.: Laboratory studies of the
933   chemical composition and cloud condensation nuclei (CCN) activity of secondary organic
934   aerosol (SOA) and oxidized primary organic aerosol (OPOA), Atmos. Chem. Phys., 11, 8913-
935   8928, 2011.

936   Lance, S., Raatikainen, T., Onasch, T., Worsnop, D., Yu, X. Y., Alexander, M. L., Stolzenburg,
937   M. R., McMurry, P. H., Smith, J. N., and Nenes, A.: Aerosol mixing-state, hygroscopic growth
938   and cloud activation efficiency during MIRAGE 2006, Atmos. Chem. Phys., 13, 5049-5062
939   2013.

940   Lanz, V. A., Alfarra, M. R., Baltensperger, U., Buchmann, B., Hueglin, C., Szidat, S., Wehrli,
941   M. N., Wacker, L., Weimer, S., Caseiro, A., Puxbaum, H., and Prevot, A. S. H.: Source
942   Attribution of Submicron Organic Aerosols during Wintertime Inversions by Advanced Factor
943   Analysis of Aerosol Mass Spectra, Environmental Science & Technology, 42, 214-220, 2008.

944   Lathem, T. L., Beyersdorf, A. J., Thornhill, K. L., Winstead, E. L., Cubison, M. J., Hecobian, A.,
945   Jimenez, J. L., Weber, R. J., Anderson, B. E., and Nenes, A.: Analysis of CCN activity of Arctic

946   aerosol and Canadian biomass burning during summer 2008, Atmos. Chem. Phys., 13, 2735-
947   2756, 2013a.

948   Lathem, T. L., Beyersdorf, A. J., Thornhill, K. L., Winstead, E. L., Cubison, M. J., Hecobian, A.,
949   Jimenez, J. L., Weber, R. J., Anderson, B. E., and Nenes, A.: Analysis of CCN activity of Arctic
950   aerosol and Canadian biomass burning during summer 2008, Atmos. Chem. Phys., 13, 2735-
951   2756, 2013b.

952   Liu, X. and Wang, J.: How important is organic aerosol hygroscopicity to aerosol indirect
953   forcing?, Environ. Res. Lett., 5, 044010, 2010.

954   Liu, Y., Brito, J., Dorris, M. R., Rivera-Rios, J. C., Seco, R., Bates, K. H., Artaxo, P., Duvoisin,
955   S., Keutsch, F. N., Kim, S., Goldstein, A. H., Guenther, A. B., Manzi, A. O., Souza, R. A. F.,
956   Springston, S. R., Watson, T. B., McKinney, K. A., and Martin, S. T.: Isoprene photochemistry
957   over the Amazon rainforest, Proceedings of the National Academy of Sciences, 113, 6125-6130,
958   2016.

959   Martin, S. T., Andreae, M. O., Althausen, D., Artaxo, P., Baars, H., Borrmann, S., Chen, Q.,
960   Farmer, D. K., Guenther, A., Gunthe, S. S., Jimenez, J. L., Karl, T., Longo, K., Manzi, A.,
961   Müller, T., Pauliquevis, T., Petters, M. D., Prenni, A. J., Pöschl, U., Rizzo, L. V., Schneider, J.,
962   Smith, J. N., Swietlicki, E., Tota, J., Wang, J., Wiedensohler, A., and Zorn, S. R.: An overview
963   of the Amazonian Aerosol Characterization Experiment 2008 (AMAZE-08), Atmos. Chem.
964   Phys., 10, 11415-11438, 2010a.

965   Martin, S. T., Andreae, M. O., Artaxo, P., Baumgardner, D., Chen, Q., Goldstein, A. H.,
966   Guenther, A., Heald, C. L., Mayol-Bracero, O. L., McMurry, P. H., Pauliquevis, T., Pöschl, U.,
967   Prather, K. A., Roberts, G. C., Saleska, S. R., Silva Dias, M. A., Spracklen, D. V., Swietlicki, E.,
968   and Trebs, I.: Sources and properties of Amazonian aerosol particles, Reviews of Geophysics,
969   48, n/a-n/a, 2010b.

970   Martin, S. T., Artaxo, P., Machado, L., Manzi, A. O., Souza, R. A. F., Schumacher, C., Wang, J.,
971   Biscaro, T., Brito, J., Calheiros, A., Jardine, K., Medeiros, A., Portela, B., Sá, S. S. d., Adachi,
972   K., Aiken, A. C., Albrecht, R., Alexander, L., Andreae, M. O., Barbosa, H. M. J., Buseck, P.,
973   Chand, D., Comstock, J. M., Day, D. A., Dubey, M., Fan, J., Fast, J., Fisch, G., Fortner, E.,
974   Giangrande, S., Gilles, M., Goldstein, A. H., Guenther, A., Hubbe, J., Jensen, M., Jimenez, J. L.,
975   Keutsch, F. N., Kim, S., Kuang, C., Laskin, A., McKinney, K., Mei, F., Miller, M., Nascimento,
976   R., Pauliquevis, T., Pekour, M., Peres, J., Petäjä, T., Pöhlker, C., Pöschl, U., Rizzo, L., Schmid,
977   B., Shilling, J. E., Dias, M. A. S., Smith, J. N., Tomlinson, J. M., Tóta, J., and Wendisch, M.:
978   The Green Ocean Amazon Experiment (GoAmazon2014/5) Observes Pollution Affecting Gases,
979   Aerosols, Clouds, and Rainfall over the Rain Forest, Bulletin of the American Meteorological
980   Society, 0, null, 2016a.

981   Martin, S. T., Artaxo, P., Machado, L. A. T., Manzi, A. O., Souza, R. A. F., Schumacher, C.,
982   Wang, J., Andreae, M. O., Barbosa, H. M. J., Fan, J., Fisch, G., Goldstein, A. H., Guenther, A.,
983   Jimenez, J. L., Pöschl, U., Silva Dias, M. A., Smith, J. N., and Wendisch, M.: Introduction:
984   Observations and Modeling of the Green Ocean Amazon (GoAmazon2014/5), Atmos. Chem.
985   Phys., 16, 4785-4797, 2016b.

986   Massoli, P., Lambe, A. T., Ahern, A. T., Williams, L. R., Ehn, M., Mikkila, J., Canagaratna, M.
987   R., Brune, W. H., Onasch, T. B., Jayne, J. T., Petaja, T., Kulmala, M., Laaksonen, A., Kolb, C.
988   E., Davidovits, P., and Worsnop, D. R.: Relationship between aerosol oxidation level and
989   hygroscopic properties of laboratory generated secondary organic aerosol (SOA) particles,
990   Geophys. Res. Lett., 37, L24801, 2010.

991   McFiggans, G., Artaxo, P., Baltensperger, U., Coe, H., Facchini, M. C., Feingold, G., Fuzzi, S.,
992   Gysel, M., Laaksonen, A., Lohmann, U., Mentel, T. F., Murphy, D. M., O'Dowd, C. D., Snider,
993   J. R., and Weingartner, E.: The effect of physical and chemical aerosol properties on warm cloud
994   droplet activation, Atmos. Chem. Phys., 6, 2593-2649, 2006.

995   Mei, F., Hayes, P. L., Ortega, A. M., Taylor, J. W., Allan, J. D., Gilman, J. B., Kuster, W. C., de
996   Gouw, J. A., Jimenez, J. L., and Wang, J.: Droplet activation properties of organic aerosols
997   observed at an urban site during CalNex-LA, J. Geophys. Res., 118, 2903-2917   2013a.

998   Mei, F., Setyan, A., Zhang, Q., and Wang, J.: CCN activity of organic aerosols observed
999   downwind of urban emissions during CARES, Atmospheric Chemistry and Physics, 13, 12155-
1000 12169, 2013b.

1001 Mikhailov, E., Vlasenko, S., Rose, D., and Pöschl, U.: Mass-based hygroscopicity parameter
1002 interaction model and measurement of atmospheric aerosol water uptake, Atmos. Chem. Phys.,
1003 13, 717-740, 2013.

1004 Moore, R. H., Bahreini, R., Brock, C. A., Froyd, K. D., Cozic, J., Holloway, J. S., Middlebrook,
1005 A. M., Murphy, D. M., and Nenes, A.: Hygroscopicity and composition of Alaskan Arctic CCN
1006 during April 2008, Atmos. Chem. Phys., 11, 11807-11825, 2011.

1007 Moore, R. H., Cerully, K., Bahreini, R., Brock, C. A., Middlebrook, A. M., and Nenes, A.:
1008 Hygroscopicity and composition of California CCN during summer 2010, J. Geophys. Res., 117,
1009 D00V12, 2012.

1010 Moore, R. H., Nenes, A., and Medina, J.: Scanning Mobility CCN Analysis—A Method for Fast
1011 Measurements of Size-Resolved CCN Distributions and Activation Kinetics, Aerosol Science
1012 and Technology, 44, 861-871, 2010.

1013 Nenes, A., Pandis, S., and Pilinis, C.: ISORROPIA: A New Thermodynamic Equilibrium Model
1014 for Multiphase Multicomponent Inorganic Aerosols, Aquatic Geochemistry, 4, 123-152, 1998.

1015 Ng, N. L., Canagaratna, M. R., Zhang, Q., Jimenez, J. L., Tian, J., Ulbrich, I. M., Kroll, J. H.,
1016 Docherty, K. S., Chhabra, P. S., Bahreini, R., Murphy, S. M., Seinfeld, J. H., Hildebrandt, L.,
1017 Donahue, N. M., DeCarlo, P. F., Lanz, V. A., Prevot, A. S. H., Dinar, E., Rudich, Y., and
1018 Worsnop, D. R.: Organic aerosol components observed in Northern Hemispheric datasets from
1019 Aerosol Mass Spectrometry, Atmos. Chem. Phys., 10, 4625-4641, 2010.

1020 Ng, N. L., Herndon, S. C., Trimborn, A., Canagaratna, M. R., Croteau, P. L., Onasch, T. B.,
1021 Sueper, D., Worsnop, D. R., Zhang, Q., Sun, Y. L., and Jayne, J. T.: An Aerosol Chemical
1022 Speciation Monitor (ACSM) for Routine Monitoring of the Composition and Mass
1023 Concentrations of Ambient Aerosol, Aerosol Sci. Technol., 45, 780-794, 2011.

1024 Pajunoja, A., Lambe, A. T., Hakala, J., Rastak, N., Cummings, M. J., Brogan, J. F., Hao, L. Q.,
1025 Paramonov, M., Hong, J., Prisle, N. L., Malila, J., Romakkaniemi, S., Lehtinen, K. E. J.,
1026 Laaksonen, A., Kulmala, M., Massoli, P., Onasch, T. B., Donahue, N. M., Riipinen, I.,
1027 Davidovits, P., Worsnop, D. R., Petaja, T., and Virtanen, A.: Adsorptive uptake of water by
1028 semisolid secondary organic aerosols, Geophys. Res. Lett., 42, 3063-3068, 2015.

1029 Park, K., Kittelson, D., Zachariah, M., and McMurry, P.: Measurement of Inherent Material
1030 Density of Nanoparticle Agglomerates, J Nanopart Res, 6, 267-272, 2004.

1031 Petters, M. D. and Kreidenweis, S. M.: A single parameter representation of hygroscopic growth
1032 and cloud condensation nucleus activity, Atmos. Chem. Phys., 7, 1961-1971, 2007.

1033 Petters, M. D., Prenni, A. J., Kreidenweis, S. M., and DeMott, P. J.: On Measuring the Critical
1034 Diameter of Cloud Condensation Nuclei Using Mobility Selected Aerosol, Aerosol Science and
1035 Technology, 41, 907-913, 2007.

1036 Pöhlker, M. L., Pöhlker, C., Klimach, T., Hrabe de Angelis, I., Barbosa, H. M. J., Brito, J.,
1037 Carbone, S., Cheng, Y., Chi, X., Ditas, F., Ditz, R., Gunthe, S. S., Kesselmeier, J., Könemann,
1038 T., Lavrič, J. V., Martin, S. T., Moran-Zuloaga, D., Rose, D., Saturno, J., Su, H., Thalman, R.,
1039 Walter, D., Wang, J., Wolff, S., Artaxo, P., Andreae, M. O., and and Pöschl, U.: Long-term
1040 observations of cloud condensation nuclei in the Amazon rain forest – Part 1: Aerosol size
1041 distribution, hygroscopicity, and new model parametrizations for CCN prediction Atmos. Chem.
1042 Phys., 16, 15709-15740, 2016.

1043 Pöschl, U., Martin, S. T., Sinha, B., Chen, Q., Gunthe, S. S., Huffman, J. A., Borrmann, S.,
1044 Farmer, D. K., Garland, R. M., Helas, G., Jimenez, J. L., King, S. M., Manzi, A., Mikhailov, E.,
1045 Pauliquevis, T., Petters, M. D., Prenni, A. J., Roldin, P., Rose, D., Schneider, J., Su, H., Zorn, S.
1046 R., Artaxo, P., and Andreae, M. O.: Rainforest aerosols as biogenic nuclei of clouds and
1047 precipitation in the Amazon, Science, 329, 1513-1516, 2010.

1048 Prenni, A. J., Petters, M. D., Kreidenweis, S. M., DeMott, P. J., and Ziemann, P. J.: Cloud
1049 droplet activation of secondary organic aerosol, J. Geophys. Res., 112, D10223, 2007.

1050 Raymond, T. M. and Pandis, S. N.: Formation of cloud droplets by multicomponent organic
1051 particles, J. Geophys. Res., 108, 4469, 2003.

1052 Reutter, P., Su, H., Trentmann, J., Simmel, M., Rose, D., Gunthe, S. S., Wernli, H., Andreae, M.
1053 O., and Poschl, U.: Aerosol- and updraft-limited regimes of cloud droplet formation: influence of
1054 particle number, size and hygroscopicity on the activation of cloud condensation nuclei (CCN),
1055 Atmospheric Chemistry And Physics, 9, 7067-7080, 2009.

1056 Rissler, J., Vestin, A., Swietlicki, E., Fisch, G., Zhou, J., Artaxo, P., and Andreae, M. O.: Size
1057 distribution and hygroscopic properties of aerosol particles from dry-season biomass burning in
1058 Amazonia, Atmos. Chem. Phys., 6, 471-491, 2006a.

1059 Rissler, J., Vestin, A., Swietlicki, E., Fisch, G., Zhou, J., Artaxo, P., and Andreae, M. O.: Size
1060 distribution and hygroscopic properties of aerosol particles from dry-season biomass burning in
1061 Amazonia, Atmos. Chem. Phys., 6, 471-491, 2006b.

Rissman, T. A., Nenes, A., and Seinfeld, J. H.: Chemical Amplification (or Dampening) of the Twomey Effect: Conditions Derived from Droplet Activation Theory, Journal of the Atmospheric Sciences, 61, 919-930, 2004.

Riva, M., Bell, D. M., Hansen, A. M. K., Drozd, G. T., Zhang, Z. F., Gold, A., Imre, D., Surratt, J. D., Glasius, M., and Zelenyuk, A.: Effect of Organic Coatings, Humidity and Aerosol Acidity on Multiphase Chemistry of Isoprene Epoxydiols, Environ. Sci. Technol., 50, 5580-5588, 2016.

Roberts, G. C., Andreae, M. O., Zhou, J., and Artaxo, P.: Cloud condensation nuclei in the Amazon Basin: "marine" conditions over a continent?, Geophysical Research Letters, 28, 2807-2810, 2001.

Roberts, G. C., Artaxo, P., Zhou, J., Swietlicki, E., and Andreae, M. O.: Sensitivity of CCN spectra on chemical and physical properties of aerosol: A case study from the Amazon Basin, Journal of Geophysical Research: Atmospheres, 107, LBA 37-31-LBA 37-18, 2002.

Rose, D., Gunthe, S. S., Mikhailov, E., Frank, G. P., Dusek, U., Andreae, M. O., and Poschl, U.: Calibration and measurement uncertainties of a continuous-flow cloud condensation nuclei counter (DMT-CCNC): CCN activation of ammonium sulfate and sodium chloride aerosol particles in theory and experiment, Atmos. Chem. Phys., 8, 1153-1179, 2008a.

Rose, D., Gunthe, S. S., Mikhailov, E., Frank, G. P., Dusek, U., Andreae, M. O., and Poschl, U.: Calibration and measurement uncertainties of a continuous-flow cloud condensation nuclei counter (DMT-CCNC): CCN activation of ammonium sulfate and sodium chloride aerosol particles in theory and experiment, Atmos. Chem. Phys., 8, 1153-1179, 2008b.

Rose, D., Nowak, A., Achtert, P., Wiedensohler, A., Hu, M., Shao, M., Zhang, Y., Andreae, M. O., and Poschl, U.: Cloud condensation nuclei in polluted air and biomass burning smoke near the mega-city Guangzhou, China - Part 1: Size-resolved measurements and implications for the modeling of aerosol particle hygroscopicity and CCN activity, Atmos. Chem. Phys., 10, 3365-3383, 2010.

Rosenfeld, D., Lohmann, U., Raga, G. B., Dowd, C. D., Kulmala, M., Fuzzi, S., Reissell, A., and Andreae, M. O.: Flood or Drought: How Do Aerosols Affect Precipitation?, Science, 321, 1309, 2008.

Schwantes, R. H., Teng, A. P., Nguyen, T. B., Coggon, M. M., Crounse, J. D., St Clair, J. M., Zhang, X., Schilling, K. A., Seinfeld, J. H., and Wennberg, P. O.: Isoprene NO3 Oxidation Products from the RO2 + HO2 Pathway, J. Phys. Chem. A, 119, 10158-10171, 2015.

Shantz, N. C., Leaitch, W. R., Phinney, L., Mozurkewich, M., and Toom-Sauntry, D.: The effect of organic compounds on the growth rate of cloud droplets in marine and forest settings, Atmos. Chem. Phys., 8, 5869-5887, 2008.

Twomey, S.: The Influence of Pollution on the Shortwave Albedo of Clouds, Journal of the Atmospheric Sciences, 34, 1149-1152, 1977.

1098 Ulbrich, I. M., Canagaratna, M. R., Zhang, Q., Worsnop, D. R., and Jimenez, J. L.: Interpretation
1099 of organic components from Positive Matrix Factorization of aerosol mass spectrometric data,
1100 Atmos. Chem. Phys., 9, 2891-2918, 2009.

1101 Vestin, A., Rissler, J., Swietlicki, E., Frank, G. P., and Andreae, M. O.: Cloud-nucleating
1102 properties of the Amazonian biomass burning aerosol: Cloud condensation nuclei measurements
1103 and modeling, Journal of Geophysical Research: Atmospheres, 112, 2007.

1104 Wang, J.: Effects of spatial and temporal variations in aerosol properties on mean cloud albedo,
1105 J. Geophys. Res., 112, D16201, 2007.

1106 Wang, J., Krejci, R., Giangrandel, S., Kuang, C., Barbosa, H. M. J., Brito, J., Carbone, S., Chi,
1107 X. G., Comstock, J., Ditas, F., Lavric, J., Manninen, H. E., Mei, F., Moran-Zuloaga, D., Pohlker,
1108 C., Pohlker, M. L., Saturno, J., Schmid, B., Souza, R. A. F., Springston, S. R., Tomlinson, J. M.,
1109 Toto, T., Walter, D., Wimmer, D., Smith, J. N., Kulmala, M., Machado, L. A. T., Artaxo, P.,
1110 Andreae, M. O., Petaja, T., and Martin, S. T.: Amazon boundary layer aerosol concentration
1111 sustained by vertical transport during rainfall, Nature, 539, 416-419, 2016a.

1112 Wang, J., Lee, Y. N., Daum, P. H., Jayne, J., and Alexander, M. L.: Effects of aerosol organics
1113 on cloud condensation nucleus (CCN) concentration and first indirect aerosol effect, Atmos.
1114 Chem. Phys., 8, 6325-6339, 2008.

1115 Wang, Q. Q., Saturno, J., Chi, X., Walter, D., Lavric, J. V., Moran-Zuloaga, D., Ditas, F.,
1116 Pohlker, C., Brito, J., Carbone, S., Artaxo, P., and Andreae, M. O.: Modeling investigation of
1117 light-absorbing aerosols in the Amazon Basin during the wet season, Atmos. Chem. Phys., 16,
1118 14775-14794, 2016b.

1119 Wex, H., Petters, M. D., Carrico, C. M., Hallbauer, E., Massling, A., McMeeking, G. R.,
1120 Poulain, L., Wu, Z., Kreidenweis, S. M., and Stratmann, F.: Towards closing the gap between
1121 hygroscopic growth and activation for secondary organic aerosol: Part 1-Evidence from
1122 measurements, Atmos. Chem. Phys., 9, 3987-3997, 2009.

1123 Whitehead, J. D., Darbyshire, E., Brito, J., Barbosa, H. M. J., Crawford, I., Stern, R., Gallagher,
1124 M. W., Kaye, P. H., Allan, J. D., Coe, H., Artaxo, P., and McFiggans, G.: Biogenic cloud nuclei
1125 in the central Amazon during the transition from wet to dry season, Atmos. Chem. Phys., 16,
1126 9727-9743, 2016.

1127 Whitehead, J. D., Gallagher, M. W., Dorsey, J. R., Robinson, N., Gabey, A. M., Coe, H.,
1128 McFiggans, G., Flynn, M. J., Ryder, J., Nemitz, E., and Davies, F.: Aerosol fluxes and dynamics
1129 within and above a tropical rainforest in South-East Asia, Atmos. Chem. Phys., 10, 9369-9382,
1130 2010.

1131 Williams, E., Rosenfeld, D., Madden, N., Gerlach, J., Gears, N., Atkinson, L., Dunnemann, N.,
1132 Frostrom, G., Antonio, M., Biazon, B., Camargo, R., Franca, H., Gomes, A., Lima, M.,
1133 Machado, R., Manhaes, S., Nachtigall, L., Piva, H., Quintiliano, W., Machado, L., Artaxo, P.,
1134 Roberts, G., Renno, N., Blakeslee, R., Bailey, J., Boccippio, D., Betts, A., Wolff, D., Roy, B.,
1135 Halverson, J., Rickenbach, T., Fuentes, J., and Avelino, E.: Contrasting convective regimes over

1136   the Amazon: Implications for cloud electrification, Journal of Geophysical Research:
1137   Atmospheres, 107, 8082, 2002.

1138   Xu, L., Guo, H. Y., Boyd, C. M., Klein, M., Bougiatioti, A., Cerully, K. M., Hite, J. R.,
1139   Isaacman-VanWertz, G., Kreisberg, N. M., Knote, C., Olson, K., Koss, A., Goldstein, A. H.,
1140   Hering, S. V., de Gouw, J., Baumann, K., Lee, S. H., Nenes, A., Weber, R. J., and Ng, N. L.:
1141   Effects of anthropogenic emissions on aerosol formation from isoprene and monoterpenes in the
1142   southeastern United States, Proc. Natl. Acad. Sci. USA, 112, 37-42, 2015a.

1143   Xu, L., Suresh, S., Guo, H., Weber, R. J., and Ng, N. L.: Aerosol characterization over the
1144   southeastern United States using high-resolution aerosol mass spectrometry: spatial and seasonal
1145   variation of aerosol composition and sources with a focus on organic nitrates, Atmos. Chem.
1146   Phys., 15, 7307-7336, 2015b.

1147   Zhang, Q., Canagaratna, M. R., Jayne, J. T., Worsnop, D. R., and Jimenez, J.-L.: Time- and size-
1148   resolved chemical composition of submicron particles in Pittsburgh: Implications for aerosol
1149   sources and processes, Journal of Geophysical Research: Atmospheres, 110, 2005.

1150   Zhang, Q., Jimenez, J. L., Canagaratna, M. R., Allan, J. D., Coe, H., Ulbrich, I., Alfarra, M. R.,
1151   Takami, A., Middlebrook, A. M., Sun, Y. L., Dzepina, K., Dunlea, E., Docherty, K., DeCarlo, P.
1152   F., Salcedo, D., Onasch, T., Jayne, J. T., Miyoshi, T., Shimono, A., Hatakeyama, S., Takegawa,
1153   N., Kondo, Y., Schneider, J., Drewnick, F., Borrmann, S., Weimer, S., Demerjian, K., Williams,
1154   P., Bower, K., Bahreini, R., Cottrell, L., Griffin, R. J., Rautiainen, J., Sun, J. Y., Zhang, Y. M.,
1155   and Worsnop, D. R.: Ubiquity and dominance of oxygenated species in organic aerosols in
1156   anthropogenically-influenced Northern Hemisphere midlatitudes, Geophys. Res. Lett., 34,
1157   L13801, 2007.

1158   Zhou, J., Swietlicki, E., Hansson, H. C., and Artaxo, P.: Submicrometer aerosol particle size
1159   distribution and hygroscopic growth measured in the Amazon rain forest during the wet season,
1160   Journal of Geophysical Research: Atmospheres, 107, LBA 22-21-LBA 22-10, 2002.

1161

1162

1163

1164 **Tables**

1165 Table 1: Density, O:C ratio and hygroscopicity associated with organic factors derived from Pos-

1166 itive Matrix Factorization (PMF) analysis. For IOP1 and IOP2, hygroscopicities of PMF organic

1167 factors were derived from time series of particle hygroscopicity under all conditions and back-

1168 ground conditions, respectively.

IOP1 (wet season)				IOP2 (dry season)			
PMF Factor	ρ (g cm^{-3})	O:C	κ	PMF Factor	ρ (g cm^{-3})	O:C	κ (Bkgd)
IEPOX-SOA	1.47	0.798	0.18±0.02	IEPOX-SOA	1.42	0.711	0.08±0.03
MO-OOA	1.80	1.19	0.20±0.02	MO-OOA	1.81	1.24	0.21±0.03
LO-OOA	1.48	0.786	0.12±0.02	LO-OOA	1.52	0.883	0.20±0.03
BBOA	1.42	0.712	0.04±0.03	Aged BBOA	1.37	0.666	0.08±0.03
Fac91	1.14	0.328	0.10±0.03	Fresh BBOA	1.23	0.536	0.00±0.07
HOA	0.95	0.163	0	HOA	1.02	0.223	0

1169
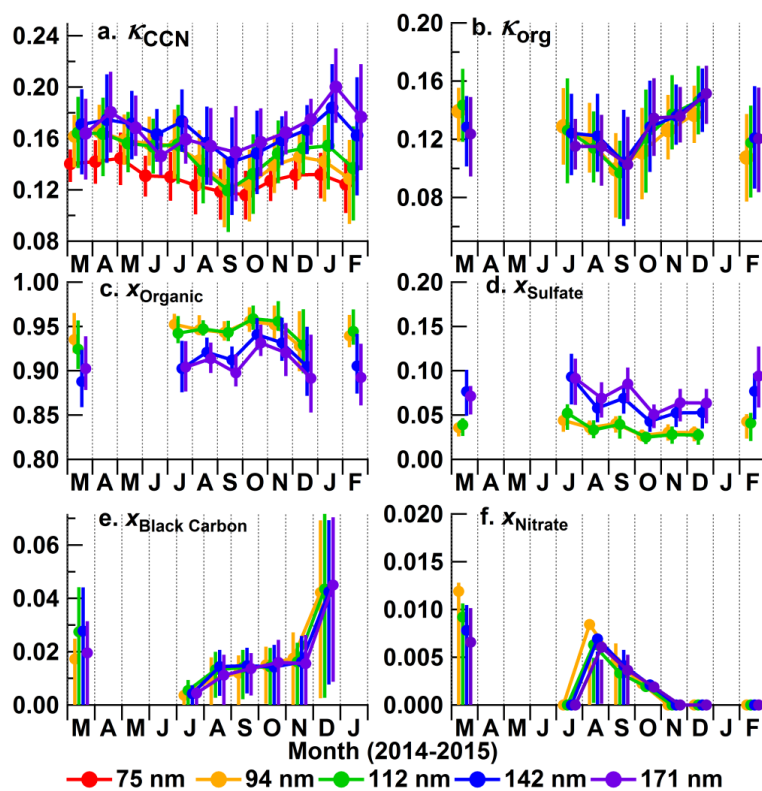
Figures

Figure 1: Seasonal variations of aerosol properties observed at the T3 site from March 2014 to March 2015, including (a) κ_{CCN}, (b) κ_{org}, and size resolved volume fraction of (c) organics, (d) sulfate, including $(NH_4)_2SO_4$ and NH_4HSO_4, (e) nitrate, and (f) refractory Black Carbon. Data points are the monthly mean; error bars represent the 25th and 75th percentiles.
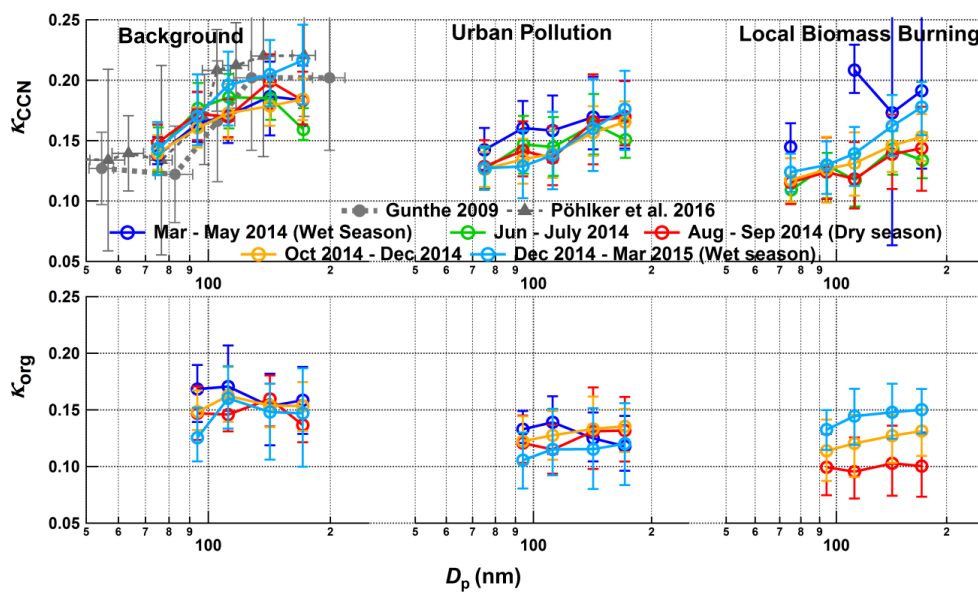
1179

1180   Figure 2: The variation of κ_{CCN} and κ_{org} with particle diameter during different seasons for each

1181   of three air mass types. Data points are the mean values; error bars are the 25 and 75 percentiles.

1182

1183

1184
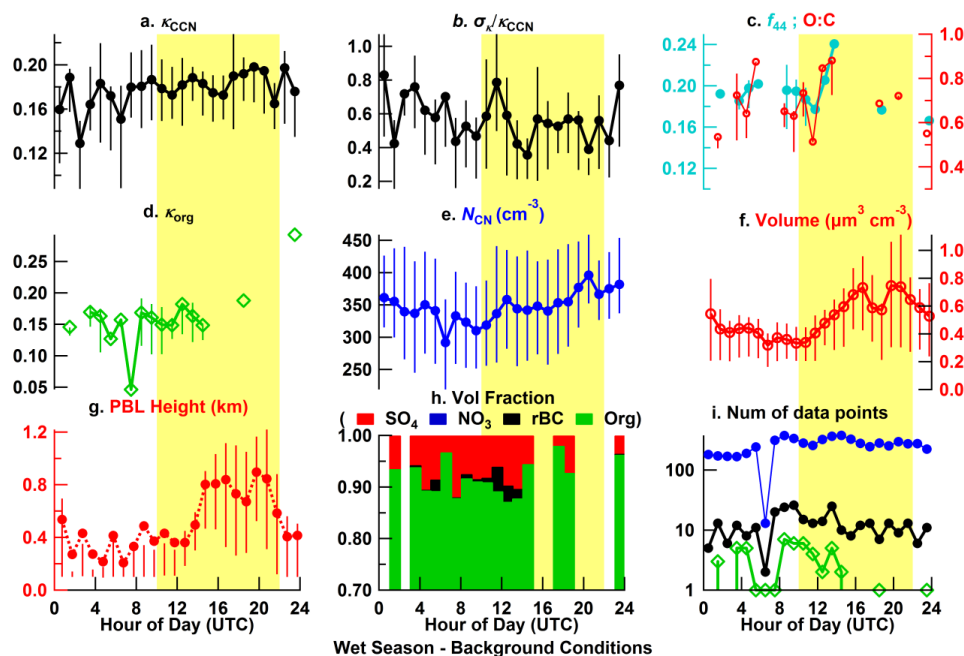
1185
1186   Figure 3: Diel variations of aerosol properties and meteorological parameter under background

1187   conditions during the wet season, including (a) κ_{CCN}, (b) $\sigma_{\kappa_{CCN}} / \overline{\kappa}_{CCN}$, (c) fraction of the organic

1188   mass at m/z = 44 (f_{44}) and the elemental ratio O:C, (d) κ_{org} derived using size resolved particle

1189   composition, (e) the total number of condensation nuclei (N_{CN}), (f) the total aerosol volume de-

1190   rived from size distribution measured by the SMPS in MAOS, (g) planetary boundary layer

1191   height as estimated using the ceilometer data, (h) the volume fractions of aerosol species, and (i)

1192   the number of samples in each hour bin corresponding to the data by the same colors and sym-

1193   bols in their respective panel. The values of κ_{CCN}, $\sigma_{\kappa_{CCN}} / \overline{\kappa}_{CCN}$, κ_{org}, and volume fraction of aero-

1194   sol species were averaged over three particle diameters of 112, 142 and 171 nm. The values of f_{44}

1195   and O:C were derived from the AMS bulk measurements. Data include the last two weeks of

1196   March 2014 when valid data from both size-resolved CCN system and AMS were available. Da-

1197   ta points are hourly averaged mean values; error bars represent the 25 and 75 percentiles of the

1198   data. Yellow shading represents the local daytime (10:00 – 22:00 UTC).
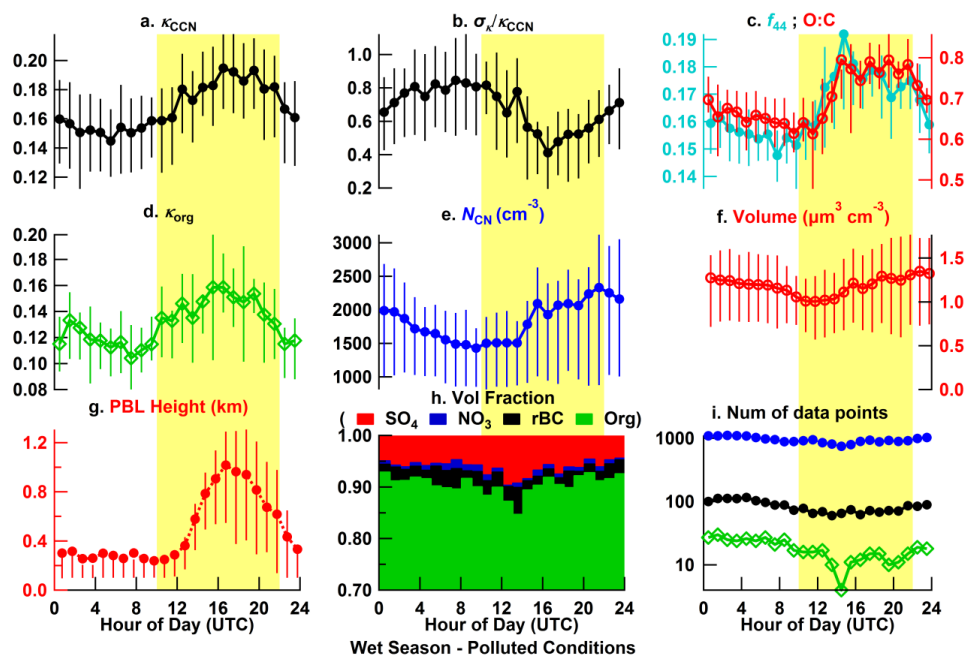
1199
1200   Figure 4: Diel variations of aerosol properties and meteorological parameters for urban pollution

1201   air masses during the wet season (analogous to Fig. 3).
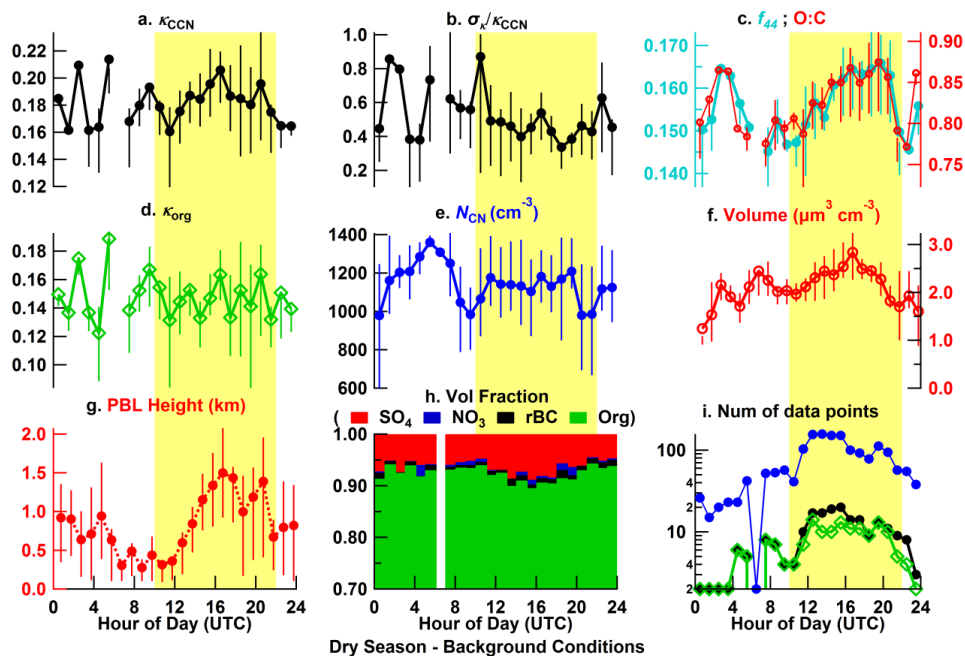
1202

Figure 5: Diel variations of aerosol properties and meteorological parameters under background

conditions during the dry season (analogous to Fig. 3).

1205

1206

1207
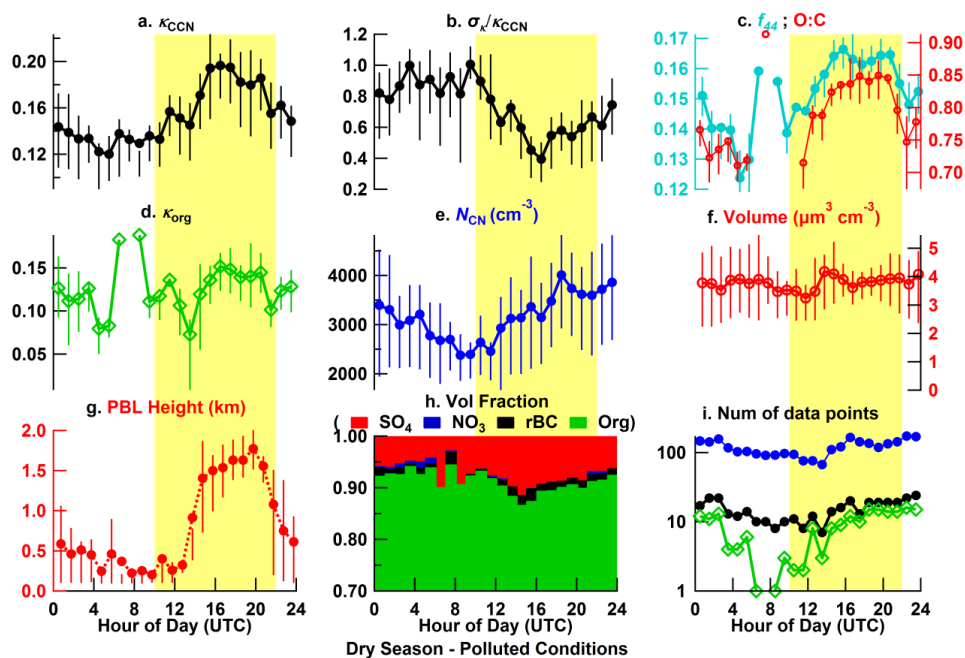
1208

1209

1210   Figure 6: Diel variations of aerosol properties and meteorological parameters for urban pollution

1211   air masses during the dry season (analogous to Fig. 3).

1212
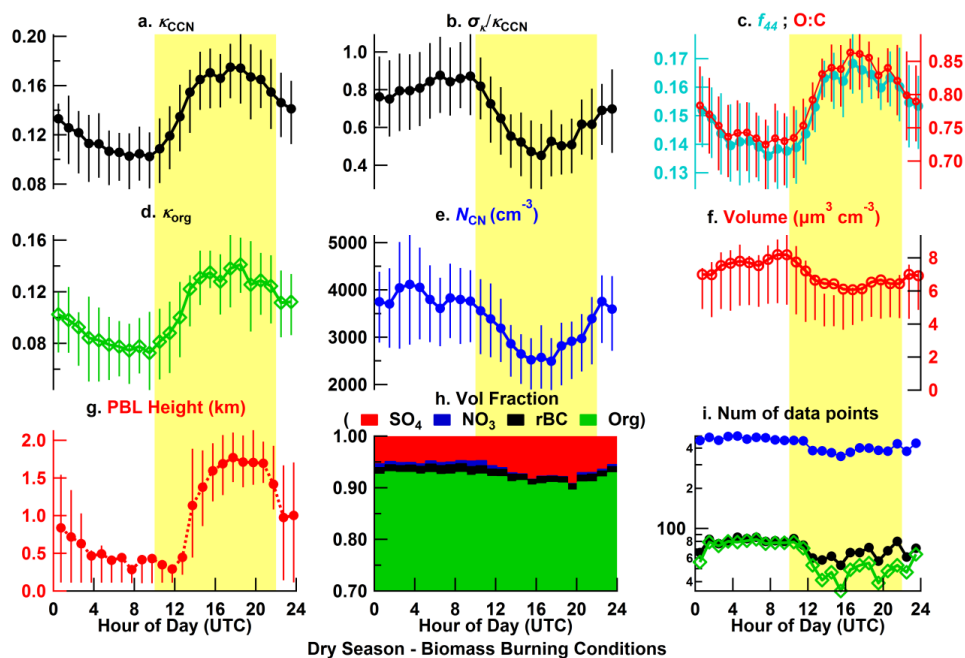
1213

1214   Figure 7: Diel variations of aerosol properties and meteorological parameters for local biomass

1215   burning air masses during the dry season (analogous to Fig. 3).

1216

1217
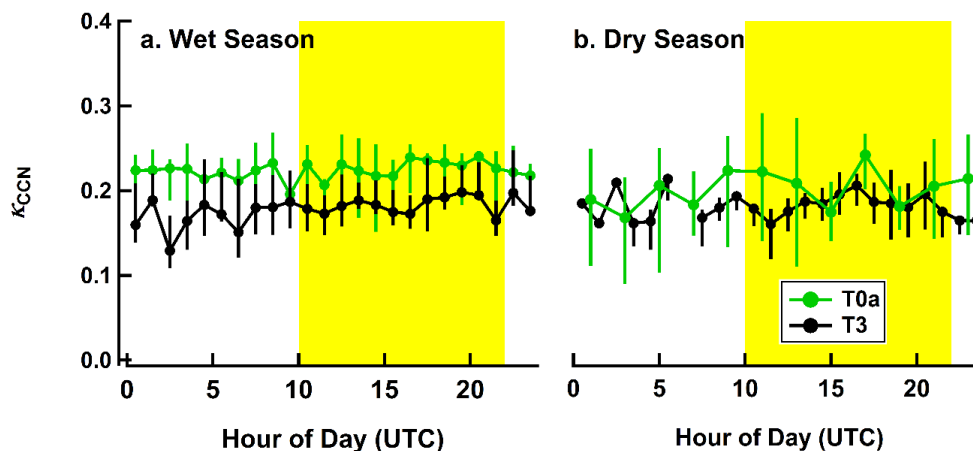
1218

1219   Figure 8: Comparison κ_{CCN} values derived from measurements at the T0a (ATTO) site (Pöhlker

1220   et al., 2016) and at the T3 site under background conditions (this study) during the (a) wet season

1221   (April and May 2014) and (b) dry season. The size resolved CCN data at T0a was collected by

1222   stepping the particle size at given CCNC supersaturations (Rose et al., 2008a). Data displayed

1223   for T0a is averaged over critical particle diameters ranging from 44 to 175 nm, while the T3 data

1224   is averaged from measurements at 112, 142, and 171 nm.

1225

1226

1227
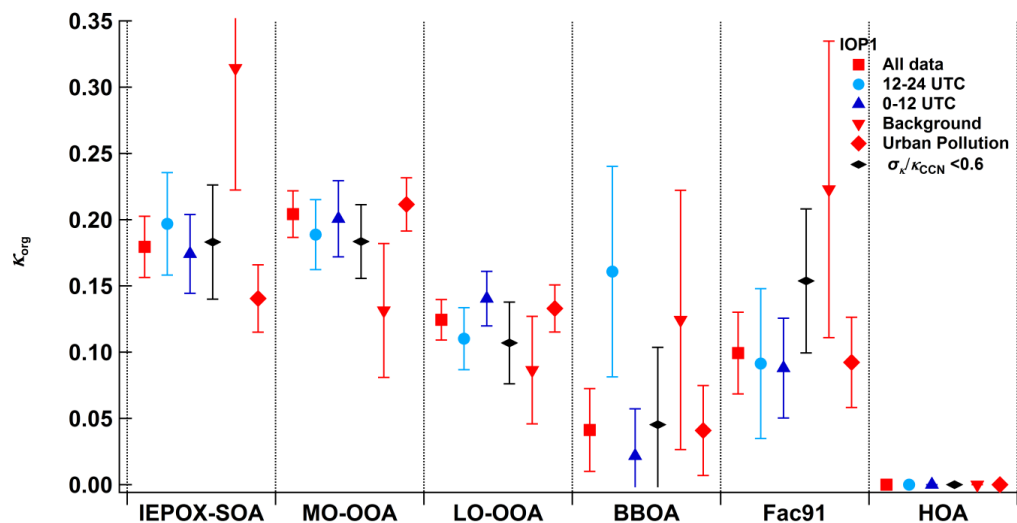
1228

1229   Figure 9: Hygroscopicity of AMS PMF factors for IOP1 (i.e., wet season) retrieved by multi-

1230   linear regressions using all data (red square), data from UTC 12:00-24:00 (cyan circle), data

1231   from UTC 0:00-12:00 (blue triangle), data under background conditions (red triangle), data un-

1232   der polluted conditions (red diamond), and data with hygroscopicity dispersion $\sigma_{\kappa_{CCN}} / \overline{\kappa}_{CCN}$ less

1233   than 0.6 (black diamond).

1234
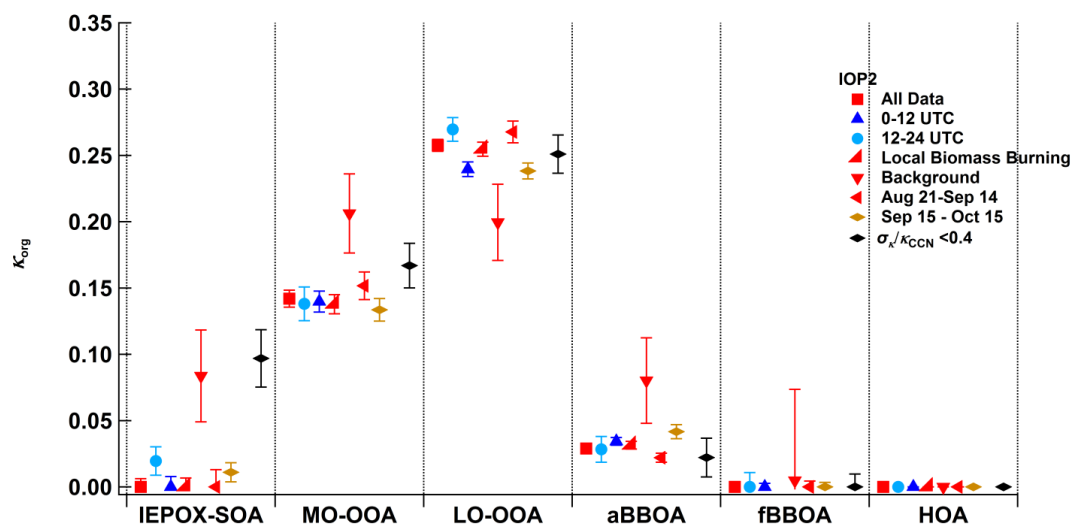
1235

1236   Figure 10: Hygroscopicity of PMF factors for IOP2 (i.e., dry season) retrieved by multi-linear

1237   regressions using all data (red square), data from UTC 12:00-24:00 (cyan circle), data from UTC

1238   0:00-12:00 (blue triangle), data with strong influence from local biomass burning (red right tri-

1239   angle), data under background conditions (red upside-down triangle), data from Aug 21 to Sep

1240   14, 2014 only (red left pointing triangle), data from Sep 15 to Oct 15 only (brown diamond), and

1241   data with a dispersion ($\sigma_{\kappa_{CCN}} / \overline{\kappa}_{CCN}$) < 0.4 (black diamond).
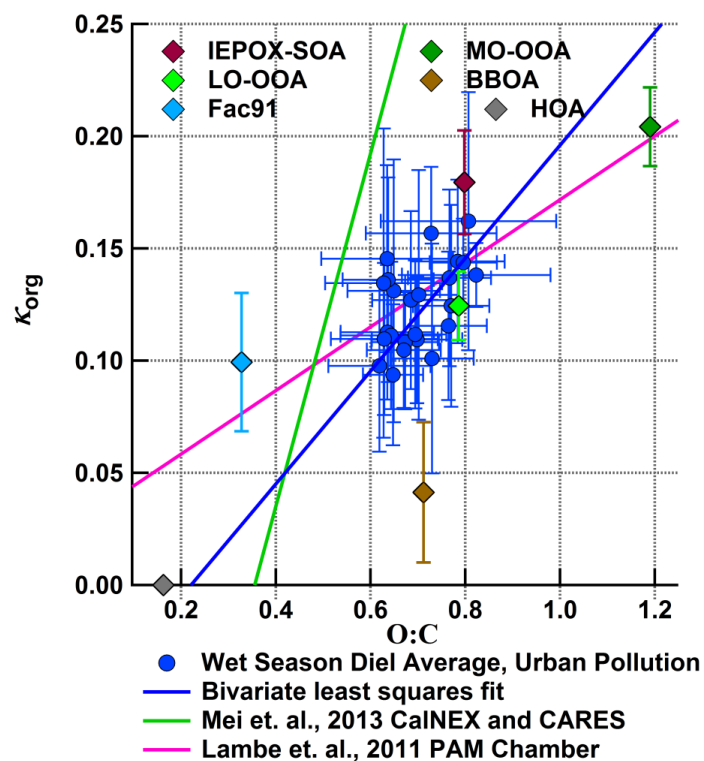
1242

Figure 11: The variation of PMF factor hygroscopicity, 1-hour diel average of organic hygrosco-

picity and O:C ratio at 142 and 171 nm for urban pollution air masses. Also shown are the rela-

tionships between κ_{org} and O:C reported by earlier field and laboratory studies.

1246

1247

1248

1249

1250

1251
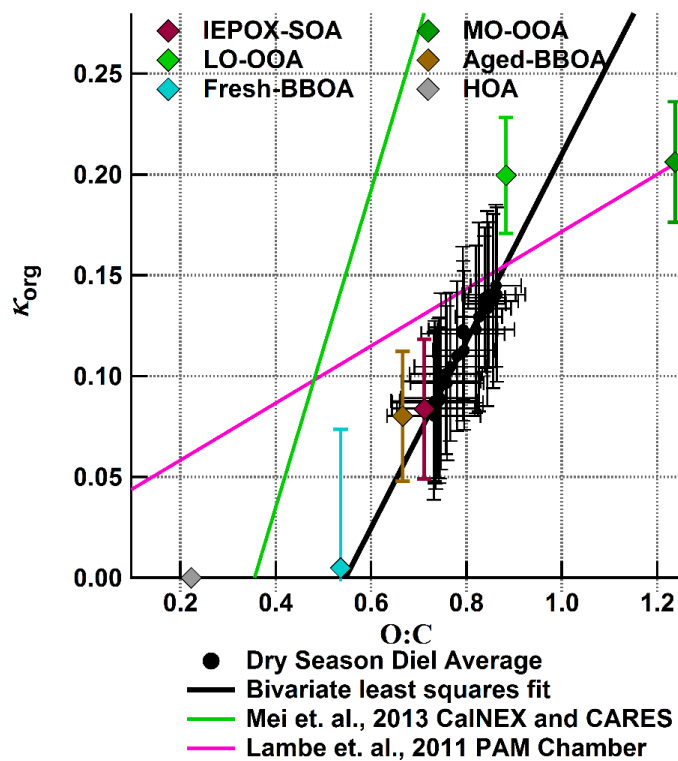
1252

1253   Figure 12: The variation of PMF factor hygroscopicity, 1-hour diel average of organic hygro-

1254   scopicity, and O:C ratio at 142 and 171 nm for local biomass burning air masses. Also shown are

1255   the relationships between κ_{org} and O:C reported by earlier field and laboratory studies.

1256